Intelligent Service Robotics (2025) 18:1315–1337
https://doi.org/10.1007/s11370-025-00646-6

ORIGINAL RESEARCH PAPER

Design exploration and kinematic validation of a transtibial prosthesis using a 2SPU-RU parallel mechanism

Victoria E. Abarca[1] · Gonzalo Oshiro[1] · Omar A. Gonzales-Huisa[1] · Dante A. Elias[1]

Received: 2 January 2025 / Accepted: 7 September 2025 / Published online: 28 September 2025

Abstract

This study presents the design exploration and kinematic validation of a transtibial prosthesis based on a 2SPU-RU parallel mechanism. The prototype is currently at Technology Readiness Level 3 (TRL 3), indicating an early-stage concept that has been evaluated under controlled conditions. The mechanism replicates dorsiflexion–plantarflexion, inversion–eversion, and abduction–adduction, corresponding to ankle motion in the sagittal, frontal, and transverse anatomic planes. The system integrates electric actuators and an ESP32 DevKit V1 microcontroller to control joint movements. Functional tests were conducted to assess kinematic performance using inertial sensors and video tracking. Additional evaluations included force distribution analysis using pressure insoles during dorsiflexion and plantarflexion, as well as energy consumption measurements across gait cycles. While the prototype demonstrates the ability to reproduce fundamental gait patterns in a suspended setup, limitations in torque, speed, and control precision restrict its current applicability. These findings provide a foundation for further development. Future work will focus on improving actuator performance, refining control strategies, and extending validation to real-world scenarios and amputee trials.

Keywords Gait analysis · Parallel mechanism · Transtibial prosthesis · Three degrees of freedom · Kinematic validation

1 Introduction

The ankle is a complex and crucial human joint, essential during walking, as it possesses the strength to support body weight and the flexibility to navigate uneven terrains [5]. Therefore, individuals with below-knee amputations who face limitations in their ability to walk may experience significant difficulties in performing daily activities, impacting them physically, psychologically, and personally, as well as affecting their family dynamics [7]. Despite prosthetic technology that has aided these individuals in regaining functional walking capabilities, most commercially available prostheses are passive and do not adequately replicate the physiological function of the ankle [11, 18]. This can lead to asymmetric gait and an increased metabolic cost of walking, which may result in long-term medical complications [18, 20]. Furthermore, inadequate dorsiflexion of the ankle increases the risk of falls on level ground and when walking on ramps [24]. Therefore, to ensure the safety and well-being of individuals with lower limb amputations, analyzing and accurately replicating ankle movements during gait in transtibial prostheses are essential.

Due to the limitations of passive prostheses, active prostheses, also known as prostheses with integrated actuators, have become a popular research topic in rehabilitation [8]. Most of these prostheses use serial mechanisms in their mechanical designs. Wang et al. [32] developed the PKU-RoboTPro, a lightweight transtibial prosthesis designed to adapt to different terrains, powered by a low-power motor to generate energy during the stance phase. The ankle model was simplified into a three-bar mechanism, representing the foot, shank, and ankle joint, along with hinges that simulate the movement of these joints. The PKU-RoboTPro can adjust the ankle impedance during stance and adapt it to different walking speeds. However, due to the lack of parallel springs or a high-power motor, it cannot provide a high assistive torque. Pană et al. [22] developed an intelligent prosthesis using magnetorheological fluids to simulate human ankle activities such as walking or running. The mechanical structure utilizes standard elements of a serial mechanism, incorporating a spherical joint based on intelligent fluids that enable up-down and lateral rotations.

✉ Victoria E. Abarca
victoria.abarca@pucp.edu.pe

[1] Biomechanics and Applied Robotics Research Laboratory, Pontificia Universidad Católica del Perú, Lima, Perú

However, a novel technology with the potential to further develop transtibial prostheses is the introduction of parallel mechanisms. Robotic assistive devices with parallel mechanisms offer superior adaptability, accuracy, high stiffness, and low inertia [36]. These mechanisms have been widely explored in various medical applications, including robotic rehabilitation devices and surgical assistance systems, due to their ability to provide precise motion control and multi-degree-of-freedom manipulation [21]. Moreover, they assist individuals with difficulties performing daily activities, giving them greater autonomy and independence [1]. In recent years, robotic exoskeletons and rehabilitation devices have seen significant advancements. For example, systems like those used for the rehabilitation of children with cerebral palsy demonstrate how parallel mechanisms can improve both biomechanical fidelity and user adaptability. These systems offer valuable insights that inform the design of prosthetic devices, particularly in enhancing mobility and improving gait dynamics during rehabilitation [26–28].

The literature shows that most research on devices using parallel mechanisms focuses on ankle rehabilitation rather than prostheses, with "U," "P," "S," "R," and "Rc" being conventional designations for the universal, prismatic, spherical, revolute, and coaxial revolute joints of the mechanisms, respectively. Zhang et al. [35] proposed the design of an ankle rehabilitation device based on the equivalent UR model. Since the actuators do not fit into narrow spaces, they utilized the 2-UPU/PRPS/[RcR][RRcR] parallel mechanism to accommodate the model. The system primarily consists of a fixed base, a moving platform, and four limbs. Li, Fan, Dong, and Rong [16] developed an ankle rehabilitation robot with a 2-UPS/RRR parallel mechanism. This mechanism comprises a fixed base, a moving platform, two UPS branched chains, and a series RRR-constrained branch. It has 3-DOF, with its three rotational axes orthogonal at a single point.

As for research on developing lower limb prostheses using parallel mechanisms, [31] developed a parallel mechanism named 2-UPR/URR with two purely rotational degrees of freedom (DOF), based on an analysis of human hip movement characteristics to assist individuals with amputations in their daily activities. The URR configuration was designated for the passive limb, while the UPR configuration was assigned as the actuating limb. Each limb of the parallel mechanism was arranged with three joints. The prosthesis demonstrated sufficient stiffness to support the human torso. Hsieh et al. [10] developed a powered ankle prosthesis with two DOF to allow movements in the sagittal and frontal planes. The mechanical design consists of two brushless electric motors, each linked to a two-stage belt drive connected to a four-bar parallel mechanism that drives the foot. Although the prosthesis has a more limited range of motion than a biological ankle due to size constraints, it provides adequate support for walking on level ground and climbing stairs. Despite these advancements, parallel mechanisms in lower limb prostheses remain relatively uncommon, highlighting a promising area for future research and development in prosthetic technology.

The electrical hardware architecture of active transtibial prostheses has evolved to meet the demands of mobility and precision. Klein and Voglewede [13] employed the Arduino Mega 2560 as the central microcontroller, selected for its compatibility and adaptability in moving prosthetic applications. For motor control, they integrated an H-Bridge motor driver, using an EMG signal as the input to the control system. The power system comprised two distinct supplies: a 9-V battery for the microcontroller and a 14.8-V, 2A battery for the motor driver. Similarly, the Ruggedized Odyssey Ankle utilizes a customized 200-W brushless DC motor, paired with a PC-104 control system and a 4400-mAh battery, to achieve a maximum ankle torque of 190 Nm [12]. Furthermore, the Proprio Foot by Ossur incorporates accelerometers and angle sensors as inputs, which are processed by a microcontroller, and features a linear actuator that enables dorsiflexion [15].

Regarding system control in transtibial prostheses, the most commonly used signals are predefined movements at 51.43%, electromyography (EMG) at 28.57%, and motion capture systems at 17.14% [32]. Klein and Voglewede [13] evaluated the implementation of a signal produced by an artificial neural network (ANN) in a stiffness controller. The ANN determines the desired ankle position and torque by receiving EMG signals and input from an encoder located at the ankle. Greene et al. [8] developed a non-backdrivable wedge cam mechanism for application in a semi-active ankle module. To control its motors, they used bang–bang control. This type of control consists of the motor receiving the maximum voltage (maximum allowed pulse width modulation (PWM) signal) when the position is outside a deadband around the desired position or receiving no voltage if it is within the desired range [10] used a proportional–derivative (PD) controller with feedforward for motor control. Full-bridge strain gauges were installed on the connectors of the four-bar parallel mechanism to measure force and provide feedback for the control system.

This study presents a transtibial prosthesis prototype that incorporates a 2SPU-RU parallel mechanism, designed to replicate ankle motion across all three anatomical planes: dorsiflexion–plantarflexion, inversion–eversion, and abduction–adduction using three actively powered degrees of freedom. Unlike previous uses of the parallel configuration in rehabilitation devices, its application in prosthetics addresses key limitations in ankle prosthesis design, such as restricted mobility, poor adaptability to uneven terrain, and limited control flexibility. This level of mobility is uncommon in current prosthetic systems, which typically offer one or two active axes. Despite its multi-axis capability, the prototype maintains a lightweight structure of just 0.5 kg (excluding

electronics), making it one of the lightest designs reported to date. The actuation system comprises two linear actuators operating under closed-loop control and a stepper motor in open-loop mode, all of which are governed by an ESP32 DevKit V1 microcontroller. As the design is currently at Technology Readiness Level 3, this study focuses on the independent kinematic evaluation of each movement in a suspended, controlled setting. Results show that the mechanism can effectively replicate fundamental gait patterns in each plane of motion. These findings establish a baseline for future development, which will aim to integrate coordinated multi-axis movement, improve actuation torque and control fidelity, and validate performance under real-world and load-bearing conditions, including trials with amputee users.

2 Methodology

2.1 Mechanical design of parallel mechanism

The robotic ankle prototype, designed as a parallel mechanism with three kinematic chains, a moving platform, a fixed base, and three actuators, was modeled in 3D and manufactured to replicate a right foot, as shown in Fig. 1. This prototype serves as a design exploration for kinematic validation, with further development planned in subsequent phases.

The parallel mechanism of the robotic ankle prototype measures 92 mm in width, 110 mm in depth, and 190 mm in height. Its design is tailored to the anthropometric measurements of a 34-year-old female user who weighs 50 kg and is 1.51 m tall.

The 2SPU-RU parallel mechanism comprises one RU kinematic chain and two SPU chains. The RU chain includes a 28BYJ-48 stepper motor (rotational joint, R), a rigid link, and a universal joint (U) connected via couplings, as depicted in Fig. 1a. Each SPU chain consists of a spherical joint (S), a prismatic joint (P) formed by an Actuonix P16-50-64-12-P linear actuator, and a universal joint (U), as illustrated in Fig. 1b.

The fixed base, a stationary component, supports two spherical joints and the 28BYJ-48 stepper motor, with contact switches on either side to limit movement, as shown in Fig. 1b. The moving platform, essential for transmitting ankle movements, integrates universal joints as part of the prosthetic mechanism, as demonstrated in Fig. 1b.

Actuation is achieved through two Actuonix P16-50-64-12-P linear actuators positioned within the SPU chains. These actuators replicate dorsiflexion–plantarflexion and inversion–eversion movements and operate using BTS7960 H-bridge drivers, as highlighted in Fig. 1b. Furthermore, the 28BYJ-48 stepper motor in the RU chain, located posteriorly, replicates abduction–adduction movements using a ULN2003 driver, as illustrated in Fig. 1a.

2.2 System architecture

Figure 2 comprehensively depicts the system architecture implemented in the 2SPU-RU parallel mechanism prototype. This diagram illustrates the interaction of matter, energy, and information within the system, highlighting their flow paths and functional roles in the system's operation.

Figure 3 illustrates the electrical and electronic architecture, detailing the power distribution and control signals assigned to each component. This includes the specification of voltage levels supplied to the elements and the communication through digital and analog signals.

The system is primarily powered by a 3-cell Li-Po battery, providing a nominal voltage of 11.1V with a capacity of 2700 mAh. This energy source powers critical components, such as the linear actuators and the stepper motor, through their corresponding drivers. Precisely, the BTS7960 drivers control the linear actuators, while the ULN2003 driver manages the operation of the stepper motor. Depending on the task requirements, these actuators generate precise movements transmitted to the moving platform, ultimately visualized as the platform's motion, which simulates foot movement.

Centralized control of the system is managed by the ESP32 DevKit v1 microcontroller, a versatile unit capable of handling multiple input and output signals. This microcontroller receives its power supply (5V) from an L7805 voltage regulator, which steps down the battery's 11.1V. The ESP32 generates PWM signals to regulate the BTS7960 drivers for the linear actuators and digital signals for the ULN2003 driver, which controls the stepper motor.

Integrating potentiometers within the linear actuators enhances the system's feedback loop. These potentiometers continuously measure the actuators' extension and transmit this position data as voltage signals to the ESP32 microcontroller. This information enables precise monitoring and real-time adjustments to ensure accurate and efficient movements.

Contact switches, which serve as mechanical sensors, manage input commands. These switches detect signals from the stepper motor, indicating specific conditions, such as the need to return the system to its initial position. The information the contact switches provide is sent to the ESP32 microcontroller, ensuring responsive and adaptive control of the mechanism.

2.3 Inverse kinematics model development

The inverse kinematics model is derived using a geometric method. This enables the calculation of actuator positions based on the moving platform's orientation, parameters, and kinematic chain analysis.

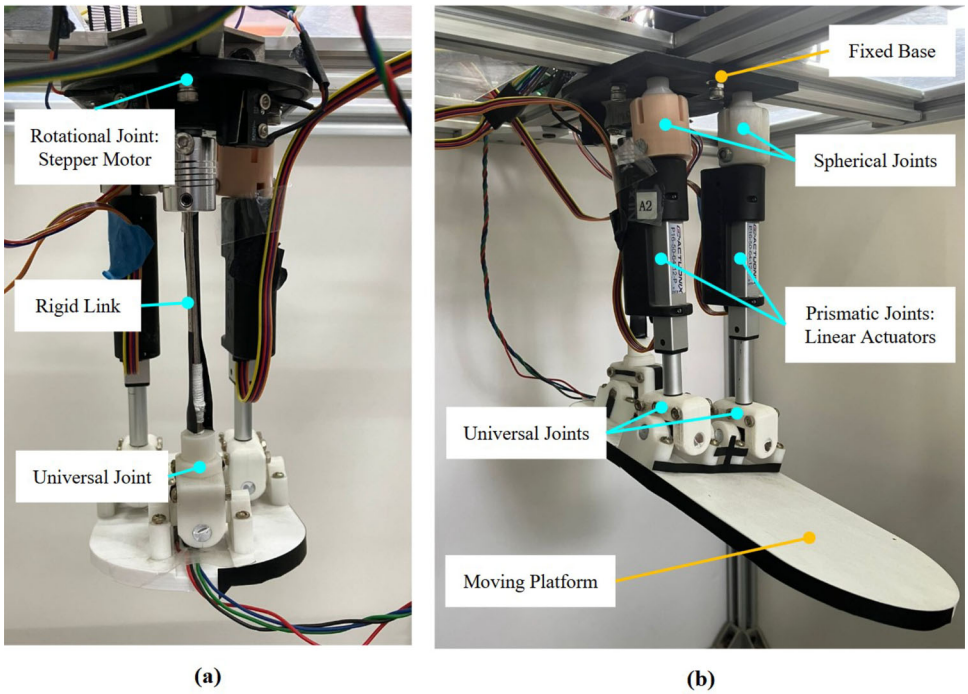

Fig. 1 2SPU-RU parallel mechanism: **a** RU kinematic chain, **b** SPU kinematic chains

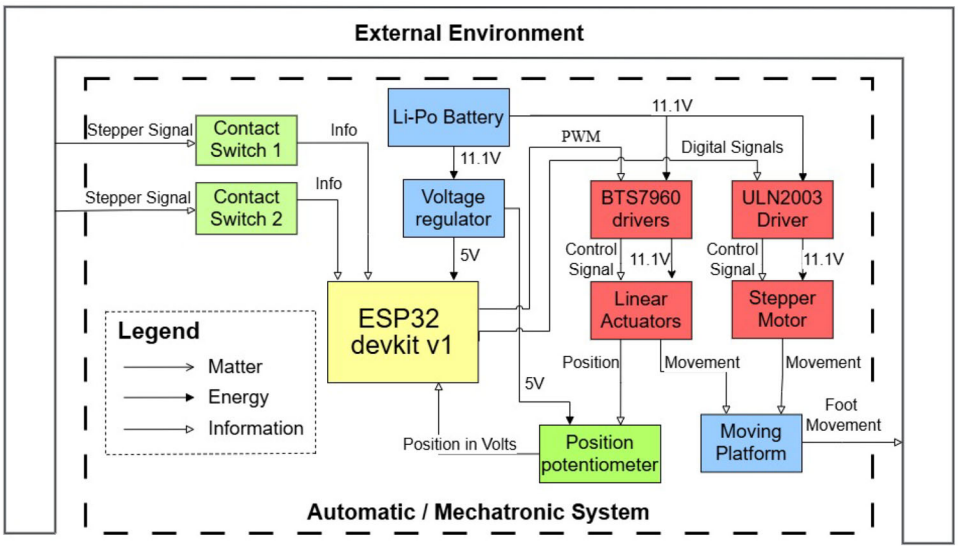

Fig. 2 System architecture

2.3.1 Parameters

Key components for the kinematic analysis include the global reference frame and relevant geometric and angular parameters, as shown in Fig. 4.

The global reference frame $O(X_0, Y_0, Z_0)$, as shown in Fig. 4a, is a fixed three-dimensional coordinate system that is essential for defining the mechanism's spatial orientation. Its origin is located at the geometric center of the fixed base, with the X_0 axis aligned anteroposteriorly to represent the primary motion during walking, the Y_0 axis positioned mediolaterally, perpendicular to the sagittal plane and parallel to the ground, and the Z_0 axis oriented vertically upward, corresponding to the body's weight vector.

The geometric parameters define the structure and kinematics of the 2SPU-RU mechanism. As shown in Fig. 4a, the linear distances between joints dictate the mechanism's configuration. The rigid triangular platforms $\Delta A_1A_2A_3$ and $\Delta B_1B_2B_3$ are isosceles and identical, with equal side lengths A_1A_2, A_1A_3, and B_1B_2, B_1B_3. The coordinates of the joints, defined in $O(X_0, Y_0, Z_0)$, determine the spatial positions and orientations of the fixed and moving components.

The angular parameters of the moving platform orientation are defined using the Bryant–Cardan $Z_pX_pY_p$ angle sequence, as illustrated in Fig. 4b. This sequence consists

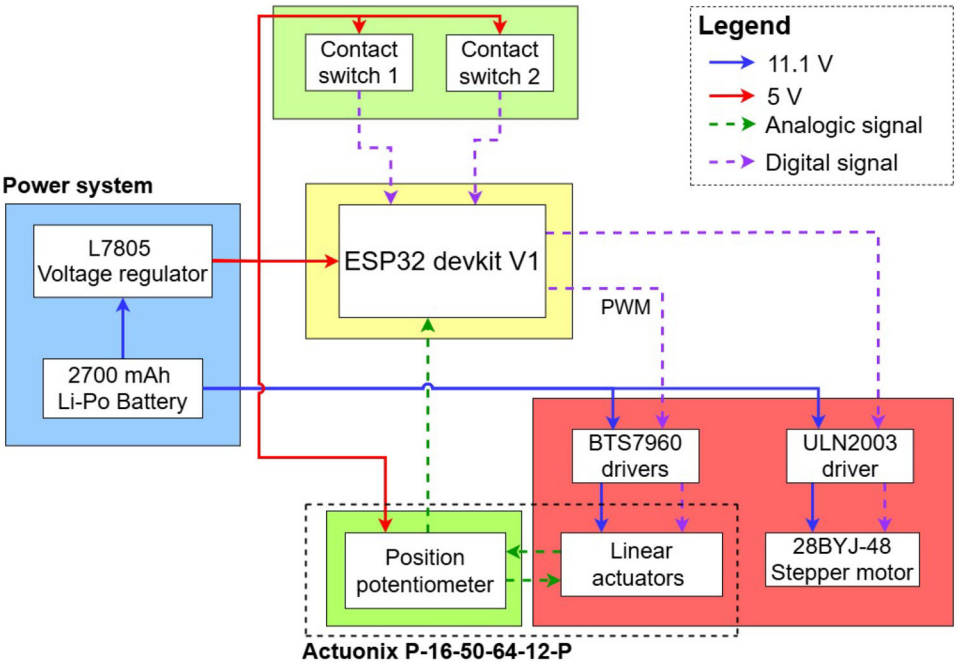

Fig. 3 Electrical–electronic architecture

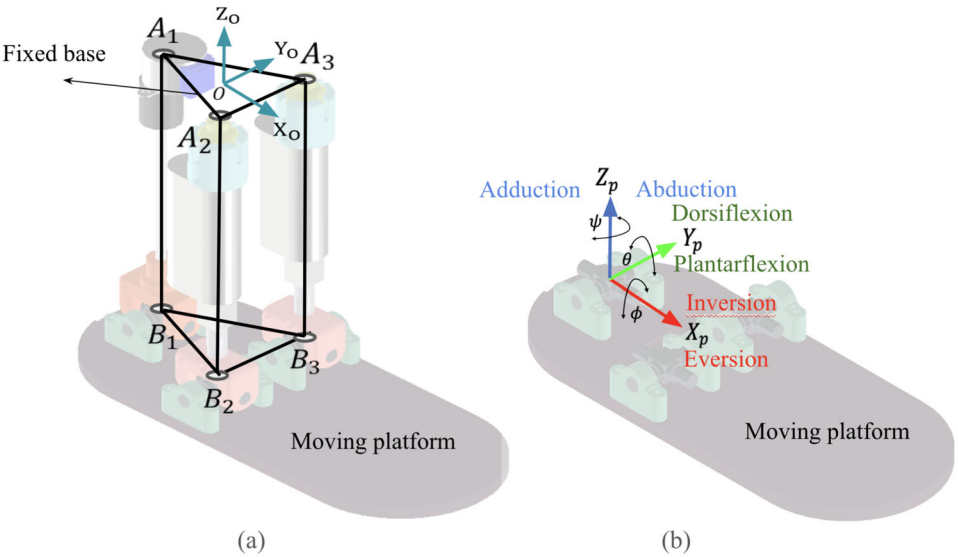

Fig. 4 Geometric parameters: **a** spatial positions, **b** spatial orientations with Bryant–Cardan angles $Z_pX_pY_p$

of a rotation ψ about the Z_p-axis, followed by a rotation ϕ about the X_p-axis, and finally a rotation θ about the Y_p-axis.

These rotations are mathematically described as Eq. (1) and Eq. (2):

$$R_{Z_pX_pY_p} = \mathrm{R}[z_p, \psi]\mathrm{R}[x_p, \phi]\mathrm{R}[y_p, \theta] \tag{1}$$

$$R_{Z_pX_pY_p} = \begin{bmatrix} -\sin\theta\sin\psi\sin\phi + \cos\theta\cos\psi & -\sin\psi\cos\phi & \sin\theta\cos\psi + \sin\psi\sin\phi\cos\theta \\ \sin\theta\sin\phi\cos\psi + \sin\psi\cos\theta & \cos\psi\cos\phi & \sin\theta\sin\psi - \sin\phi\cos\theta\cos\psi \\ -\sin\theta\cos\phi & \sin\phi & \cos\theta\cos\phi \end{bmatrix} \tag{2}$$

The angular velocity $\boldsymbol{\omega}_p$ of the moving platform is derived from the time variation of the rotation matrix $R_{Z_pX_pY_p}$ (Eq. (2)), obtained Eq. (3).

$$\boldsymbol{\omega}_p = \begin{bmatrix} \omega_{px} \\ \omega_{py} \\ \omega_{pz} \end{bmatrix} = \begin{bmatrix} 0 & \cos\psi & -\sin\psi\cos\theta \\ 0 & \sin\psi & \cos\psi\cos\theta \\ 1 & 0 & \sin\theta \end{bmatrix} \begin{bmatrix} \dot{\psi} \\ \dot{\theta} \\ \dot{\phi} \end{bmatrix} \tag{3}$$

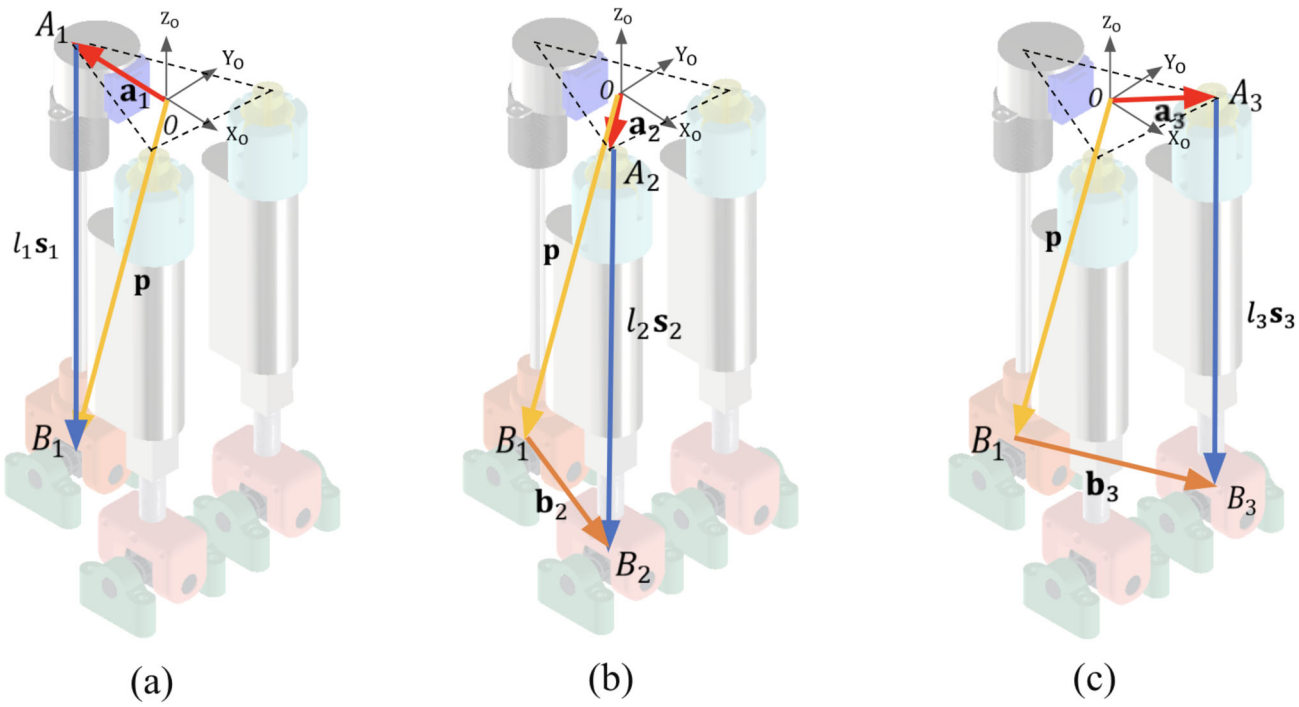

Fig. 5 Kinematic chains of the parallel mechanism: **a** RU chain vectors (first chain), **b** SPU chain vectors (second chain), **c** SPU chain vectors (third chain)

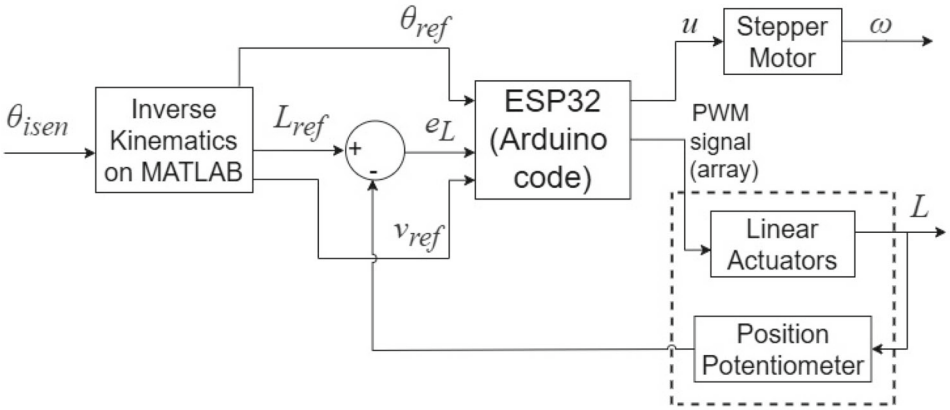

Fig. 6 Control system diagram of the robotic ankle joint prototype

2.3.2 Kinematic analysis

The kinematic analysis of the three chains in the parallel mechanism focuses on their position and velocity vectors, as shown in Fig. 5.

The RU kinematic chain is defined relative to the fixed coordinate system $O(X_0, Y_0, Z_0)$. As shown in Fig. 5a, the position vector equation for this chain is expressed as Eq. (4).

$$\mathbf{a}_1 + l_1\mathbf{s}_1 = \mathbf{p} \tag{4}$$

where $\mathbf{a}_1$ locates joint A_1, $l_1\mathbf{s}_1$ represents the rotary actuator, and $\mathbf{p}$ indicates point P. Since the vector magnitude is constant, the derivative $\dot{\mathbf{l}}_1 = 0$. The actuator rotation ω_1 corresponds to $\dot{\psi}$, which is the first intrinsic rotation in the rotation matrix $R_{Z_pX_pY_p}$.

The SPU kinematic chains are analyzed using the position vector equation shown in Fig. 5b, c and Eq. (5).

$$\mathbf{a}_2 + l_2\mathbf{s}_2 = \mathbf{p} + \mathbf{b}_2, \quad \mathbf{a}_3 + l_3\mathbf{s}_3 = \mathbf{p} + \mathbf{b}_3 \tag{5}$$

where $\mathbf{a}_2$ and $\mathbf{b}_2$ locate joints A_2 and B_2. Also, $\mathbf{a}_3$ and $\mathbf{b}_3$ locate joints A_3 and B_3. The magnitude and direction of the vectors are determined as Eq. (6) and Eq. (7).

$$l_2 = |\mathbf{p} + \mathbf{b}_2 - \mathbf{a}_2|, \quad l_3 = |\mathbf{p} + \mathbf{b}_3 - \mathbf{a}_3|. \tag{6}$$

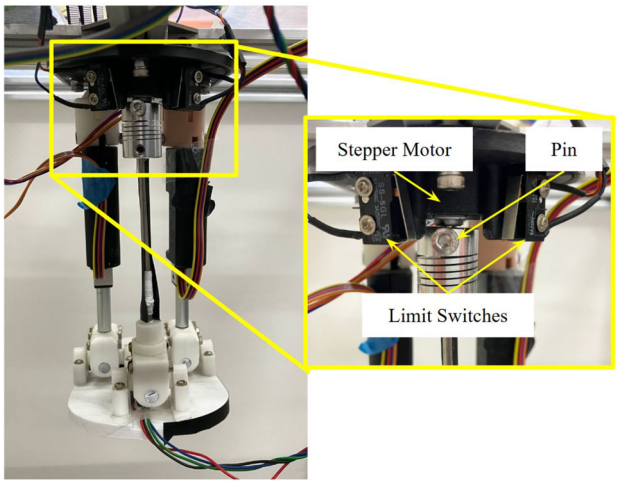

Fig. 7 Rear-front view of the robotic ankle prototype

$$\mathbf{s}_2 = \frac{\mathbf{p} + \mathbf{b}_2 - \mathbf{a}_2}{l_2}, \quad \mathbf{s}_3 = \frac{\mathbf{p} + \mathbf{b}_3 - \mathbf{a}_3}{l_3}. \tag{7}$$

The velocity of joint B_2 and B_3 is computed using Eq. (8).

$$\mathbf{V}_{B_2} = \mathbf{V}_p + \boldsymbol{\omega}_p \times \mathbf{b}_2, \quad \mathbf{V}_{B_3} = \mathbf{V}_p + \boldsymbol{\omega}_p \times \mathbf{b}_3 \tag{8}$$

where $\mathbf{V}_{B_2}$ is the velocity of B_2, $\mathbf{V}_{B_3}$ is the velocity of B_3, $\mathbf{V}_p$ is the velocity of the moving platform, $\boldsymbol{\omega}_p \times \mathbf{b}_2$ and $\boldsymbol{\omega}_p \times \mathbf{b}_3$ represent the velocity contribution to angular motion.

2.4 Control system

The control system diagram is presented in Fig. 6. The control system variables are defined as follows:

- θ_{isen} represents the ankle joint angles derived from gait test data collected from female participants. These data were obtained from the study conducted by [2].
- θ_{ref} represents the reference angle for the stepper motor rotation.
- L_{ref} denotes the reference length for the linear actuators.
- v_{ref} indicates the reference speed.
- u represents the voltage signal required for the stepper motor to rotate according to the reference angle.
- The PWM signal (array) indicates the extension length for the linear actuators in a format interpretable by the driver.
- ω denotes the rotational speed of the stepper motor, observable during abduction–adduction movements.
- L represents the extension length of the linear actuators, observable during dorsiflexion–plantarflexion and inversion–eversion movements.

Based on the inverse kinematics calculations previously explained, a code was developed in MATLAB v.2023a to calculate the lengths and velocities of the actuators required to extend or retract during the ankle's trajectory. For each ankle movement (dorsiflexion–plantarflexion, inversion–eversion, and abduction–adduction), two position vectors and two velocity vectors were generated for the linear actuators alongside an angular position vector for the stepper motor. The results are generated as vectors and subsequently used as input in a code implemented in Arduino IDE.

The ESP32 DevKit V1 microcontroller was programmed to control the prototype using Arduino IDE. In the dorsiflexion–plantarflexion and inversion–eversion movements, which depend exclusively on the linear actuators, an empirical conversion function was established that relates the actuator length (0 to 50 mm) to 12-bit values (0 to 2047). This conversion is necessary to compare the reference position with the actual position, which is measured using a potentiometer integrated into the actuators.

To allow some tolerance when comparing the actual position with the reference position, a "deadband" was implemented. When the actual position falls within the accepted range, the system advances to the next position and velocity vector, ensuring a smooth transition between positions with defined speed.

The abduction–adduction movement depends on the 28BYJ-48 stepper motor, which is programmed in "half-step" mode to follow up to 8 phases at a speed of 24 RPM. Unlike the linear actuators, the stepper motor operates in an open-loop control system, lacking feedback. The program's input is the reference angular position vector for the stepper motor. As the motor's movement is angular, the system calculates the necessary angular displacement after the initial setup.

To ensure accurate positioning, the stepper motor must first be returned to its initial position. This is achieved by using two limit switches on either side of the motor, and a pin aligned perpendicularly to the motor shaft, as shown in Fig. 7. The microcontroller rotates the motor until the pin touches one of the switches, after which it rotates by a predefined angle to reach the initial position. This method ensures the motor starts at the correct position before initiating any movement.

2.5 Kinematics testing with the prototype

The objective of the present study is to conduct functional tests with the physical prototype of the robotic ankle, which features the 2SPU-RU parallel mechanism. These tests were designed to evaluate the kinematic performance of the prosthesis, using the angular ranges obtained across three planes of ankle motion during gait as a reference for generating the angular motion trajectories of the robotic ankle prototype.

The movements evaluated were dorsiflexion–plantarflexion in the sagittal plane, inversion–eversion in the frontal plane, and abduction–adduction in the horizontal plane. Each movement was analyzed separately using videogrammetry and Kinovea v0.9.5 software. A dedicated test environment was set up, as shown in Fig. 8, where the prototype was suspended in air on an aluminum frame. Acrylic plates were installed on the frame to house the electronic circuits and system components.

As reference markers for the video software, black adhesive tape was applied in a line pattern on the prototype, as shown in Fig. 9, to facilitate Kinovea analysis. The Arduino IDE code, referenced in Section 2.4, guided the ankle prototype along the reference angular trajectory. Five gait cycles were recorded for each movement in its respective plane. Once the recordings were completed, the videos were processed using Kinovea v0.9.5 software with the "Get Angle" tool, which tracked the angles generated during each gait cycle.

Figure 10 illustrates the procedure used to measure the angles. The recorded data were then exported to CSV files for further analysis. Following the extraction of CSV files, the data were analyzed using Python. Each CSV file contained multiple gait cycles for the three evaluated movements. For the analysis, one representative gait cycle from each movement was selected. This selected gait cycle was then converted into a percentage of time to facilitate the evaluation of the gait cycle phases for each movement. To visualize the results, the selected gait cycle for each movement was plotted alongside the corresponding reference trajectory, allowing for a comparison between the recorded angular movement of the physical prototype and the expected reference movement. These results are presented in Results Section.

2.5.1 Error calculation methodology

Two error metrics, Root Mean Square Error (RMSE) and Dynamic Time Warping (DTW), are employed to evaluate the accuracy of the simulated movement compared to the original movement. These methods comprehensively compare the original and simulated dorsiflexion–plantarflexion, inversion–eversion, and abduction–abduction trajectories over a gait cycle. The results help assess how closely the robotic ankle prototype replicates the expected movements.

RMSE is a widely used metric to quantify the differences between predicted and observed values. It is susceptible to more significant deviations, making it suitable for assessing the accuracy of the simulated angles. RMSE is defined as Eq. (9).

$$\text{RMSE} = \sqrt{\frac{1}{n}\sum_{i=1}^{n}(y_i - \hat{y}_i)^2}, \tag{9}$$

where y_i represents the observed values, $\hat{y}_i$ represents the simulated values, and n is the total number of data points. RMSE penalizes more significant errors than smaller ones, making it a robust choice for error analysis when the data distribution is Gaussian [4].

DTW is an algorithm that measures similarity between two sequences that may vary in time or speed. Unlike RMSE, DTW accounts for temporal shifts and optimizes the sequences by minimizing the cumulative alignment cost. The DTW distance is calculated using dynamic programming and is defined as Eq. (10).

$$D(i,j) = d(x_i, y_j) + \min \begin{cases} D(i-1, j), & \text{Insertion} \\ D(i, j-1), & \text{Deletion} \\ D(i-1, j-1), & \text{Match} \end{cases}, \tag{10}$$

where $d(x_i, y_j)$ is the local distance between the i-th point in the original sequence and the j-th point in the simulated sequence and $D(i, j)$ is the cumulative cost. The optimal alignment path is determined by finding the path with the minimum cumulative cost, ensuring that the two sequences are compared effectively [14].

Therefore, RMSE was chosen because it provides a direct measure of deviation, emphasizing larger errors that could indicate significant discrepancies in gait replication. DTW was selected for its ability to handle temporal misalignments, common in human gait analysis. The combination of these metrics provides a robust assessment of the magnitude and temporal differences between the original and simulated patterns.

2.6 Experimental procedure using pressure insoles

The XSENSOR Intelligent Insole system and XSENSOR Pro Foot & Gait software were used to acquire force and pressure data during the dorsiflexion–plantarflexion movement, specifically to evaluate the ground interaction of the robotic ankle prototype. This testing was conducted as part of the initial validation of the prototype to assess its kinematic performance during key phases of gait. The testing protocol consisted of two stages:

1. **Prototype testing**: Assessing the force distribution generated by the robotic ankle prototype.
2. **User testing**: Capturing real gait force data from the same participant used for previous inertial sensor-based kinematic data collection.

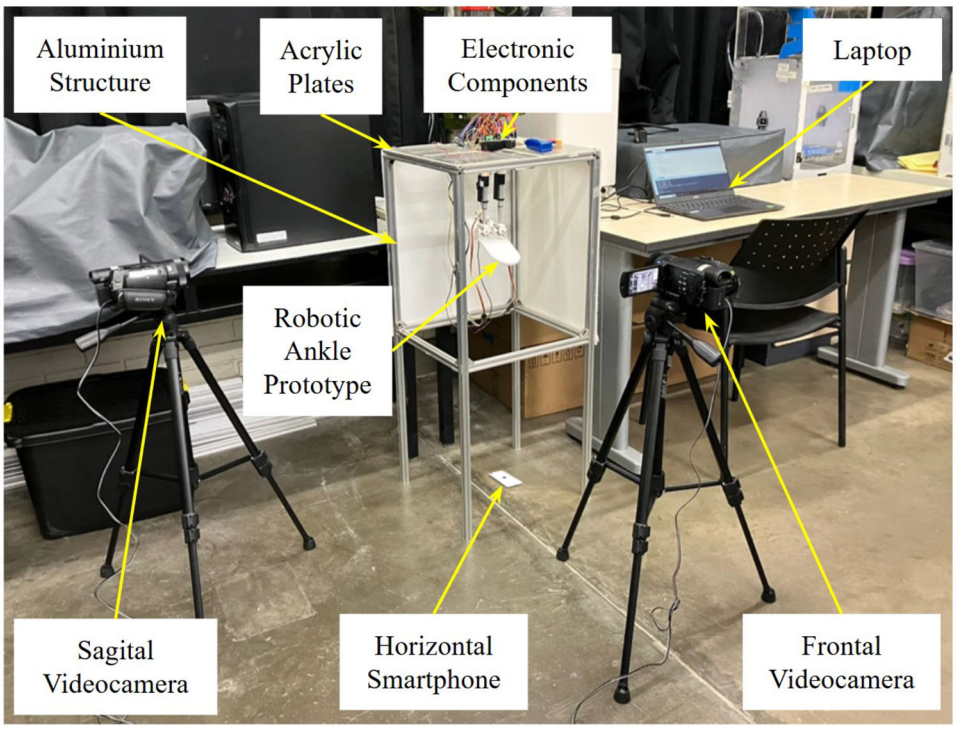

Fig. 8 Recording setup configuration. Two cameras, SONY FDR-AX700, were positioned perpendicular to the sagittal and frontal planes. For the movements in the horizontal plane, a smartphone was used and positioned perpendicularly to the plane

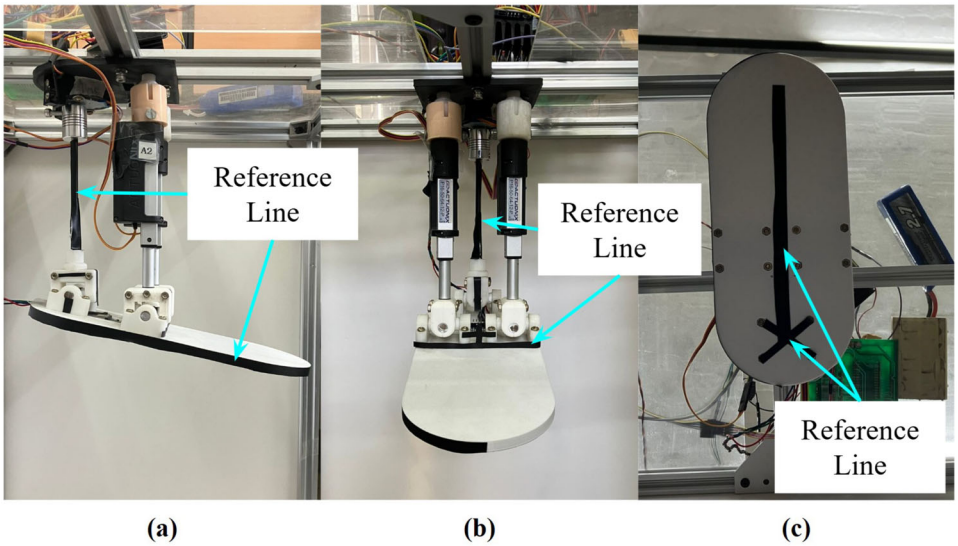

Fig. 9 Views of the prototype with black adhesive tape in **a** the sagittal plane, **b** the frontal plane, and **c** the horizontal plane

2.6.1 Robotic ankle prototype testing

For prototype testing, the device was placed over the pressure insoles to measure the force exerted on the ground during dorsiflexion and plantarflexion. To simulate realistic gait conditions, the prosthesis was manually lifted during the swing phase of the gait cycle. Additionally, a 1.5 kg load was applied to the heel to simulate a more realistic force distribution. The setup is shown in Fig. 11, and the total weight of the prototype, including this load, was assumed to be 2 kg for force normalization purposes.

2.6.2 User testing

For comparison, a human gait trial was conducted using the same participant who provided the kinematic reference data. The pressure insoles were inserted into the participants' footwear, and force and pressure data were recorded while they walked at a self-selected speed. The participant's body weight, 53.5 kg, was used for force normalization.

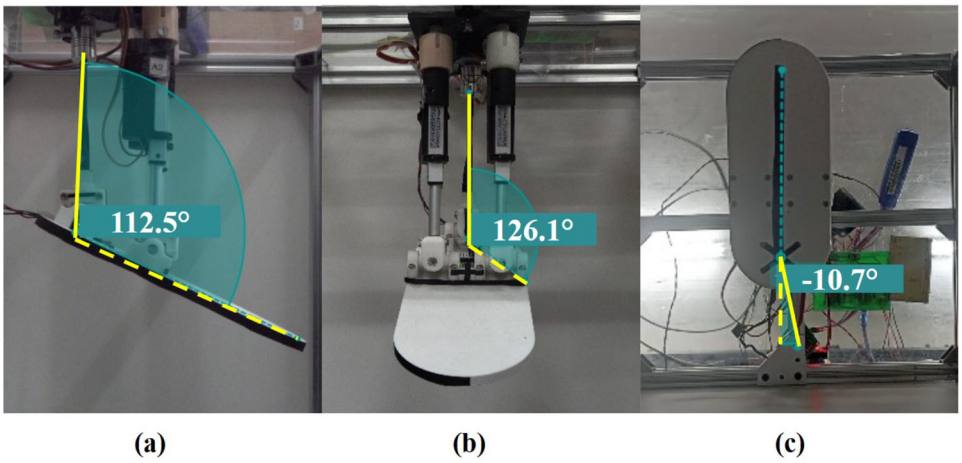

Fig. 10 Use of the "Get Angle" tool in Kinovea v0.9.5 for **a** dorsiflexion–plantar flexion movement in the sagittal plane, **b** inversion–eversion movement in the frontal plane, and **c** abduction–adduction movement in the horizontal plane

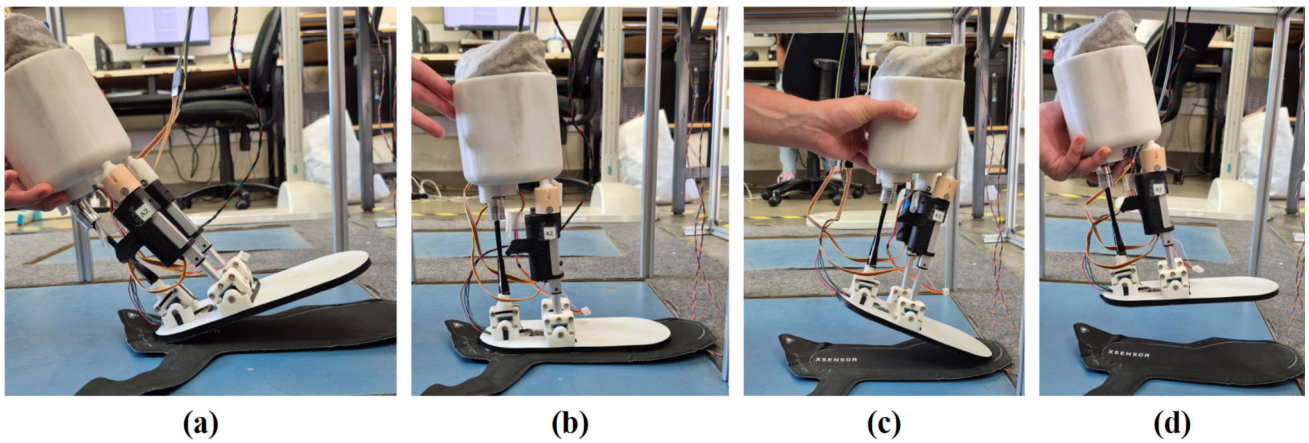

Fig. 11 Robotic ankle prototype testing using pressure insoles: **a** initial contact, **b** midstance, **c** toe-off, **d** swing phase

2.6.3 Normalization and data comparison

A weight-normalized force approach was applied to ensure a valid comparison between the forces generated by the robotic prototype and those recorded by the human participant. The force values were expressed as a percentage of total body weight using Eq. (11):

$$F_{\text{normalized}} = \frac{F_{\text{measured}}}{mg} \tag{11}$$

where mg represents the subject's body weight (53.5 kg) or the prototype's total weight (2 kg). This normalization enables a direct comparison of force distribution, regardless of absolute weight differences.

2.7 Early-stage energy consumption analysis

At this TRL 3 stage, the objective is not to optimize power usage but to verify that the chosen actuators can complete representative gait cycles within the capacity of a readily available battery. Energy consumption was therefore measured in a single-degree-of-freedom (DoF) manner for the three primary ankle motions: dorsiflexion–plantarflexion, inversion–eversion, and abduction–adduction. The prototype was powered from an 11.1-V, 2700-mAh Li-Po pack. A precision digital multimeter, placed in series with the supply, recorded the average current (I) while each DoF executed one complete gait cycle. All tests were repeated three times, and the results were averaged.

Electrical power in a DC circuit is given by $P = V \times I$, where V is the supply voltage and I is the measured current. Integrating that power over the measured cycle duration t yields the total electrical work performed by the actuators, as shown in Eq. (12):

$$E = P \times t, \tag{12}$$

Energy may be reported either in joules (J) or, for battery-sizing purposes, converted to milliampere-hours using Eq. (13):

$$E_{(\text{mAh})} = \frac{E_{(\text{J})}}{V} \frac{1}{3600} \tag{13}$$

These values provide a first-order indication that the present battery comfortably supports laboratory testing with a margin for firmware overhead. A detailed duty-cycle study, together with comparisons against commercial powered ankles, is deferred to future TRL 4-5 iterations when the mechanical and control architectures have stabilized.

2.8 Early-stage reliability screening

A theoretical reliability screening was conducted to obtain an order-of-magnitude estimate of electronic component failure rates. Calculations followed the MIL-HDBK-217F parts-count method, which expresses the failure rate (λ) (in FIT, failures per 10^9 hours) as stated in Eq. (14):

$$\lambda_{\text{total}} = \lambda_b \cdot \pi_T \cdot \pi_A \cdot \pi_Q \cdot \pi_E \cdot \pi_S \cdots \tag{14}$$

with λ_b the base rate and π factors accounting for temperature, application stress, quality, environment, etc. Assuming moderate laboratory conditions ($\pi \approx 1$) and series configuration of the electronics, the system-level reliability over a mission time T is shown in Eq. (15):

$$R(T) = exp(-\lambda_{\text{total}} \times T) \tag{15}$$

The resulting figures indicate a high theoretical mean-time-between-failure for bench testing; however, this model does not account for mechanical wear, connector fretting, lubricant degradation, or seal fatigue. Experimental lifetime cycling and high-accelerated life testing will be conducted on the TRL5 prototype once the final actuator and gearbox selections are finalized.

2.9 Torque estimation for the actuation system

The torque estimation was performed exclusively for the dorsiflexion–plantarflexion movement, representing the most critical and biomechanically significant motion during the gait cycle. Dorsiflexion–plantarflexion is responsible for ground clearance during the swing phase and propulsion in the stance phase, making it a key determinant of gait functionality. In contrast, inversion–eversion and abduction–adduction contribute more to balance and stability than propulsion, so this study did not prioritize their torque analysis.

Since the robotic ankle prototype does not incorporate embedded torque sensors, the torque exerted by the actuators was estimated based on manufacturer specifications. The force generated by each Actuonix P16-50-64-12-P linear actuator was obtained from its datasheet, which lists a maximum force of 90 N for the 64:1 gear ratio configuration. The torque was calculated using Eq. (16):

$$\tau = F \times r \tag{16}$$

where τ is the torque (Nm), $F = 90N$ is the actuator force, and $r = 0.06m$ is the perpendicular distance from the actuator attachment point to the ankle rotation axis. This results in a torque of 5.4 Nm for dorsiflexion–plantarflexion movement.

It is essential to note that this estimated torque is lower than the typical human ankle torque, which ranges from 30 to 60 Nm during dorsiflexion–plantarflexion, depending on walking speed and load. This limitation stems from the force capabilities of the selected actuators. The prototype operates within these constraints as part of an early-stage evaluation, and future iterations will seek to incorporate higher-torque actuators or enhance the mechanical design to replicate human-like torque values more accurately.

3 Results

This section presents the results for dorsiflexion–plantarflexion, inversion–eversion, and abduction–adduction movements of the robotic ankle prototype during a gait cycle, compared with reference data from a gait study [2]. The gait cycle is divided into the stance phase (65%) and the swing phase (35%).

The stance and swing phases are divided into five and three subphases, respectively, resulting in eight subphases within the gait cycle. The stance phase begins with the initial contact (IC) subphase at 0% of the gait cycle, followed by the loading response (LR) subphase, which spans from 0% to 10%. Next is the midstance (MSt) subphase, which covers 10% to 30%, followed by the terminal stance (TSt) subphase, from 30% to 55%. The stance phase concludes with the pre-swing (PSw) subphase, which occurs from 55% to 65%.

Conversely, the swing phase begins with the initial swing (ISw) subphase, which occurs between 65% and 75% of the gait cycle. This is followed by the mid-swing (MSw) subphase, covering 75% to 85%. Finally, the gait cycle concludes with the terminal swing (TSw) subphase, occurring from 85% to 100%.

3.1 Dorsiflexion–plantarflexion

For the dorsiflexion–plantarflexion movement, a comparative graph was created to analyze the performance of the robotic ankle prototype against the reference gait cycle movement, as shown in Fig. 12a. The linear actuators control this movement exclusively, operating synchronously throughout the gait cycle. The length of the actuators during the cycle is shown in Fig. 12b.

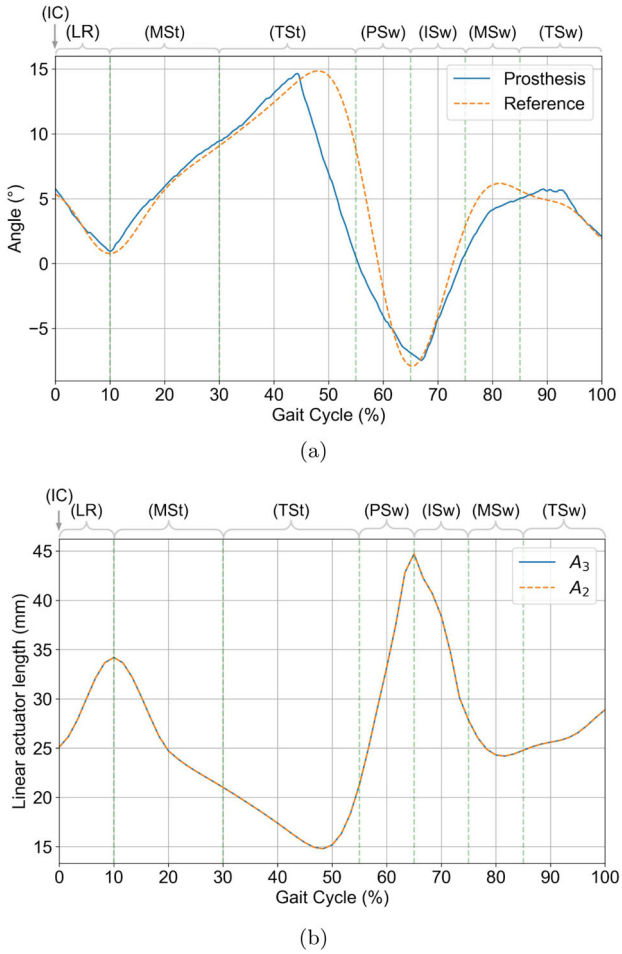

Fig. 12 Dorsiflexion–plantarflexion movement in the sagittal plane during gait cycle: **a** comparative graph between the robotic ankle prototype and reference movement of the gait cycle, **b** graph of linear actuator A_2 and A_3 extension/retraction during dorsiflexion–plantarflexion movement. Subphase: initial contact (IC), midstance (MSt), terminal stance (TSt), pre-swing (PSw), initial swing (ISw), mid-swing (MSw), terminal swing (TSw)

The gait cycle begins with the stance phase. During the first subphase, initial contact, both actuators are extended to approximately 25 mm, corresponding to an angle of 5°. In the following subphase, loading response, the actuators extend further, reaching a length of approximately 34 mm, which results in an angle of 1°. During midstance and part of terminal stance, the actuators retract to a length of approximately 15 mm, reaching a peak at 43% of the gait cycle, with a maximum angle of approximately 15°. Subsequently, in the second part of the terminal stance and pre-swing, the actuators reach their maximum extension during the cycle, with a length of 45 mm, which occurs at approximately 68% of the gait cycle.

The swing phase begins with the initial swing, where the actuators retract. During mid-swing, the retraction continues but at a slower rate, reaching a length of 25 mm. Finally, in the terminal swing subphase, the actuators extend again to approximately 27 mm before returning to the initial position (initial contact), marking the start of a new gait cycle.

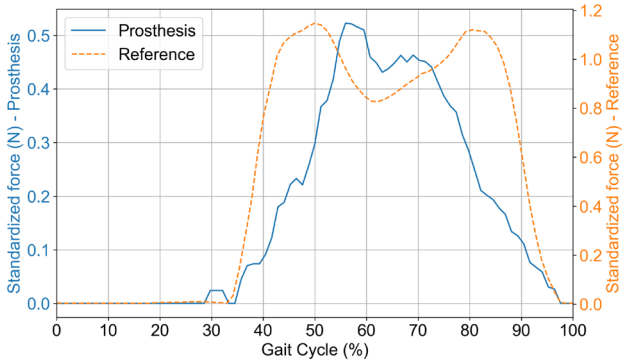

Fig. 13 Robotic ankle prototype testing using pressure insoles: **a** initial contact, **b** midstance, **c** toe-off, **d** swing phase

The estimated torque generated by the actuators during dorsiflexion–plantarflexion was 5.4 Nm, considering a maximum actuator force of 90 N and a lever arm distance of 6 cm. This theoretical value offers insight into the system's mechanical capabilities, but it does not account for dynamic effects or variations resulting from actuator speed limitations.

During the dorsiflexion–plantarflexion movement, the system operated at an average current of 0.5 A with a supply voltage of 11.1 V, resulting in a power consumption of 5.55 W. Given that each gait cycle lasts 11.1 s, the energy consumed per cycle is 61.605 J. Converting this energy into milliampere-hours (mAh) yields approximately 1.54 mAh per cycle. Since a gait cycle occurs roughly 324 times per hour (3600 s / 11.1 s), the system draws about 500 mAh per hour. Consequently, with a battery capacity of 2700 mAh at 11.1 V, the system would operate continuously for approximately 5.4 h, highlighting the high energy demand of the actuators during this movement.

3.1.1 Ground interaction analysis

In addition to the kinematic and energetic evaluations performed with the robotic ankle prototype in a suspended setup, an experimental assessment of its ground interaction was conducted using pressure insoles.

This test compared the force distribution generated by the prototype during dorsiflexion–plantarflexion against that of a human user. Figure 13 presents the overlaid normalized estimated force graphs for a complete gait cycle of the robotic ankle prototype and the user.

A comparison of the force values reveals a difference in the peak amplitude between the prototype and the user. The prototype exhibits a maximum peak value of 0.52, whereas the user's force data reach a peak of 1.2.

The overall shape of the curve is similar in both cases. The force remains at 0 when either the prototype or the user's foot is in the air, followed by a peak when the heel makes contact with the ground. This is followed by a valley during the foot-flat phase and a second peak during toe-off before returning to 0 as the foot leaves the ground.

These results provide insight into the prototype's ability to replicate human-like force distribution during dorsiflexion–plantarflexion. However, differences in peak force suggest limitations due to weight and load-bearing capacity.

3.2 Inversion–eversion

Figure 14a compares the inversion–eversion movement between the robotic ankle prototype and the recorded movement of the female user. This movement is controlled exclusively by the linear actuators, which operate alternately as shown in Fig. 14b. The gait cycle begins with the stance phase, starting with the initial contact subphase, where actuator A_2 is extended to 37.5 mm and actuator A_3 is extended to 34.5 mm, forming an angle of 4°.

During the loading response and midstance subphases, actuator A_2 extends while actuator A_3 retracts, reaching a peak at approximately −0.5° at 25% of the gait cycle. At the end of the midstance subphase, both actuators reverse their direction, and this pattern is maintained throughout the terminal stance, pre-swing, initial swing, and part of the mid-swing subphase. In mid-swing, a peak of approximately 7° is reached at 80% of the gait cycle, with actuator A_2 extended to 40 mm and A_3 to 32 mm. Finally, the actuators switch direction again (A_2 extends and A_3 retracts), maintaining this pattern throughout the remainder of the mid-swing and terminal swing subphase, completing the gait cycle.

In addition to evaluating the kinematic behavior of the robotic ankle prototype, the power consumption associated with the inversion–eversion movement was analyzed. The system consumed an average current of 0.42 A at a supply voltage of 11.1 V, resulting in a power consumption of 4.66 W. With a gait cycle duration of 1.07 s, the energy consumed per cycle is 4.99 J. Converting this energy into milliampere-hours (mAh) yields approximately 0.125 mAh per cycle. Given that a gait cycle occurs about 3364 times per hour (3600 s/1.07 s ≈ 3364), the system would draw roughly 419 mAh per hour. Therefore, with a battery capacity of 2700 mAh, the inversion–eversion movement could be sustained continuously for approximately 6.44 h, underscoring the lower energy demand of the actuators during this movement compared to dorsiflexion–plantarflexion.

3.3 Abduction–adduction

Figure 15 compares the abduction-adduction movement between the robotic ankle prototype and the recorded movement of the female user. This movement is controlled solely by the stepper motor labeled A1. The stance phase begins with the initial contact subphase at 0°. During the loading response and part of the midstance subphase, the stepper motor rotates clockwise, forming an angle of approximately 5° at 20% of the gait cycle.

The stepper motor then reverses to counterclockwise rotation, maintaining this direction through the remainder of midstance and part of terminal stance, peaking at approximately 9° at 47% of the gait cycle. For the rest of the terminal stance and during the pre-swing subphase, the stepper motor rotates clockwise, returning the prototype to its initial position of 0° at 65% of the gait cycle.

Once more, the stepper motor reverses counterclockwise during the initial swing and mid-swing subphases, reaching an angle of 7° at 85% of the gait cycle. Finally, during the ter-

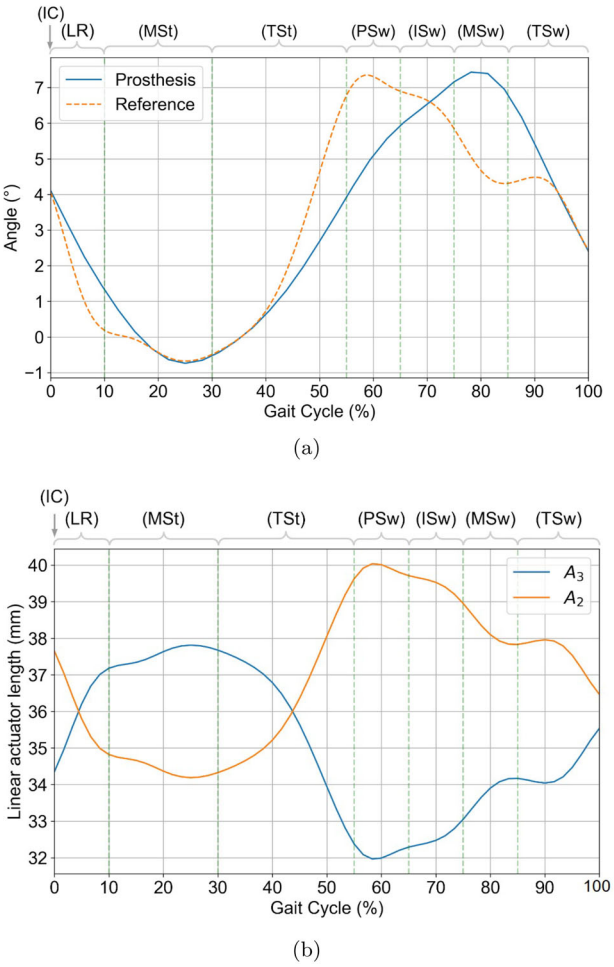

Fig. 14 Inversion–eversion movement in the frontal plane during a gait cycle: **a** comparative graph between the robotic ankle prototype and reference movement of the gait cycle, **b** graph of linear actuator A_2 and A_3 extension/retraction during inversion–eversion movement. Subphase: initial contact (IC), midstance (MSt), terminal stance (TSt), pre-swing (PSw), initial swing (ISw), mid-swing (MSw), terminal swing (TSw)

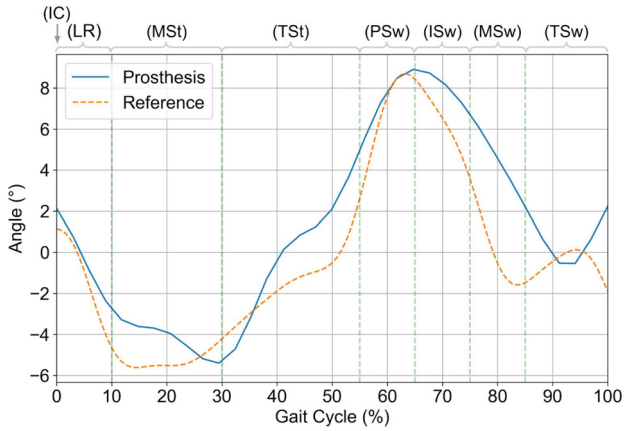

Fig. 15 Comparative graph of abduction-adduction in the horizontal plane between the robotic ankle prototype and the female user's recorded movement during a gait cycle. Subphase: initial contact (IC), midstance (MSt), terminal stance (TSt), pre-swing (PSw), initial swing (ISw), mid-swing (MSw), terminal swing (TSw)

minal swing subphase, the motor rotates clockwise, bringing the prototype back to its initial position of 0° and preparing it for the start of a new gait cycle.

In addition to evaluating the kinematic characteristics of the robotic ankle prototype, the power consumption during the abduction–adduction movement was analyzed. The system required an average current of 0.16 A at a supply voltage of 11.1 V, yielding a power consumption of 1.94 W. With a gait cycle lasting 1.52 s, the energy consumed per cycle is 2.95 J. Converting this to milliampere-hours results in approximately 0.074 mAh per cycle. Given that about 2368 cycles occur per hour (3600 s/1.52 s), the hourly consumption is roughly 175 mAh, suggesting that, with a 2700 mAh battery, the abduction–adduction movement could be sustained continuously for approximately 15.4 h. This lower power demand aligns with the movement's mechanical simplicity, primarily driven by a stepper motor.

3.4 Reliability estimation of the electronic system

We assume that components operate under moderate conditions (room temperature), so most correction factors are unity except where explicitly noted. For a system where components are arranged in series, the overall failure rate is approximated as the sum of each component's individual failure rates (λ_{total}).

Table 1 presents the failure rate calculations for each system component, following the MIL-HDBK-217F standard. The values include the base failure rate (λ_b) and relevant correction factors ($\pi_T, \pi_A, \pi_Q, \pi_E, \pi_S$). The total system failure rate is obtained by summing the failure rates of all components.

Assuming a mission time of $T = 1000$ hours, the reliability of each component is calculated using (17):

$$R(T) = \exp\left(-\lambda_{\text{total}} \times 10^{-9} \times T\right) \tag{17}$$

For instance, the ESP32 microcontroller has a failure rate of 100 FIT, and its reliability over 1000 h is:

$$\begin{aligned} R_{\text{ESP32}} &= \exp\left(-100 \times 10^{-9} \times 1000\right) \\ &\approx \exp(-0.0001) \approx 0.99990. \end{aligned}$$

Similarly, the reliability of each component in Table 1 can be computed. Since the system follows a series configuration, the overall system reliability is given by (18):

$$\begin{aligned} R_{\text{system}}(T) &\approx \exp\left(-\left(\sum \lambda_{\text{total}}\right) \times 10^{-9} \times T\right) \\ &= \exp\left(-1740 \times 10^{-9} \times 1000\right) \\ &\approx \exp(-0.00174) \approx 0.99826, \end{aligned} \tag{18}$$

indicating an overall system reliability of 99.83% over 1000 h.

4 Discussion

4.1 Dorsiflexion–plantarflexion movement

The root mean square error (RMSE) for dorsiflexion–plantarflexion motion was 2.621, and the dynamic time warping (DTW) distance was 32.803, indicating moderate temporal misalignment between the original and simulated patterns (Fig. 16). Despite these deviations, the prosthetic system replicates the essential phases and overall motion trends of dorsiflexion within the gait cycle.

Analysis of actuator behavior throughout the gait cycle (Fig. 12) reveals effective tracking of key subphases, including initial contact, loading response, midstance, and terminal stance. However, the timing of retraction and extension peaks differs slightly from the user's natural motion. For instance, the first retraction peak occurs at 43% of the gait cycle in the prototype, compared to 48% in the user. These deviations are attributed to limitations in actuator speed and load-handling capacity.

The estimated actuator torque of 5.4 Nm is considerably lower than the typical human ankle torque range of 30–60 Nm, limiting the prototype's ability to reproduce realistic force output. Additionally, while the selected linear actuators can achieve speeds up to 18 mm/s without load, their effective operational speed decreases under working conditions. This affects both motion accuracy and timing, contributing

Table 1 Failure rate calculation for system components using MIL-HDBK-217F

Component	λ_b (FIT)	π_T	π_A	π_Q	π_E	π_S	λ_{total} (FIT)
ESP32 DevKit V1	100	1.0	1.0	1.0	1.0	–	100
Actuonix P16-50-64-12-P	200	1.0	1.0	1.0	1.0	1.1	220
28BYJ-48 Stepper Motor	500	1.0	1.0	1.0	1.0	–	500
ULN2003 Driver	200	1.0	1.0	1.0	1.0	–	200
BTS7960 Driver	500	1.0	1.0	1.0	1.0	–	500
L7805 Voltage Regulator	200	1.0	1.0	1.0	1.0	–	200
Capacitor (0.33 μF)	10	1.0	1.0	1.0	1.0	–	10
Capacitor (0.1 μF)	10	1.0	1.0	1.0	1.0	–	10
System total							1740

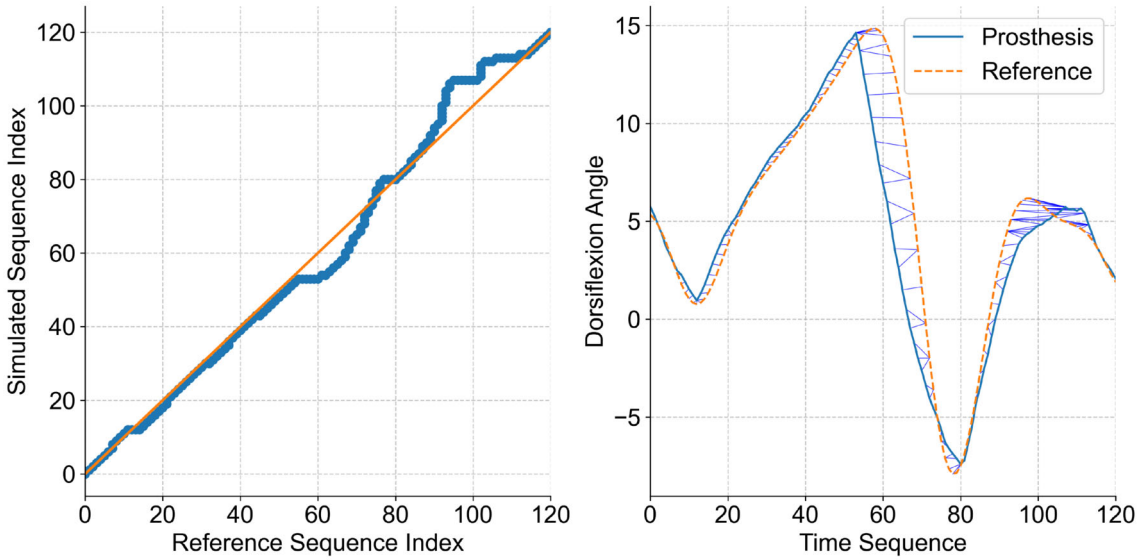

Fig. 16 Warping path, sequence, and alignment for dorsiflexion–plantarflexion. Blue circle, warping path; red straight line, diagonal of the matrix; blue line, alignment

to a prolonged gait cycle duration of 11.1 s compared to the approximately 1-second cycle of natural human gait. Nevertheless, the system captures the principal kinematic features of ankle movement within the exploratory scope of this early-stage prototype.

The focus on dorsiflexion–plantarflexion in this study is justified by its dominant role in stance propulsion and swing clearance during gait. Although inversion–eversion and abduction–adduction contribute to ankle stability, their torque demands are lower and more variable, depending on external conditions. Future work could address these additional degrees of freedom for a more comprehensive evaluation.

4.1.1 Evaluation of ground interaction performance

Force analysis using pressure insoles revealed that, although the overall shape of the force curve was preserved, the peak amplitude differed between the user (1.2) and the robotic prototype (0.52). This difference stems from the prototype's lower weight and the absence of full-body dynamics, which naturally increase ground reaction forces in human locomotion.

Despite this amplitude discrepancy, both curves exhibited similar temporal patterns: minimal force during swing, a peak at heel strike, a valley in midstance, and a second peak at toe-off. This suggests the prototype successfully reproduces the general force distribution associated with gait phases.

A key limitation is that the prototype was only evaluated for dorsiflexion–plantarflexion. Human ankles also exhibit inversion–eversion and abduction–adduction movements, which are essential for maintaining stability on uneven terrain. The absence of these movements could affect real-world performance.

The reduced force output also correlates with the system's limited torque capacity, as previously discussed. Furthermore, actuator speed constraints contribute to minor timing

mismatches in peak force events, reinforcing the need for actuators with greater speed and load capacity.

In summary, while the robotic ankle replicates essential force and motion patterns, enhancements in torque output, actuator speed, and multi-plane mobility are necessary to improve the fidelity of ground interaction and functional realism. Future iterations could explore stronger actuators, mechanical amplifiers, or adaptive control strategies to address these limitations.

4.2 Inversion–eversion movement

The RMSE for inversion–eversion was 1.359, and the DTW distance for eversion was 8.954, indicating strong alignment between the original and simulated trajectories (Fig. 17). The warping path closely follows the diagonal, reflecting minimal temporal and magnitude deviations. The actuators accurately replicate the first angular peak at approximately 25% of the gait cycle, closely matching the user's recorded movement (Fig. 14). These results highlight the prototype's effectiveness in reproducing lateral ankle behavior during gait.

Despite this satisfactory performance, some limitations remain. During loading response, midstance, and swing subphases, the user's ankle exhibits subtle directional changes that the prototype does not fully capture, resulting in a smoother, less nuanced trajectory. This simplification stems from the prototype's mechanical constraints and the limited degrees of freedom offered by the two linear actuators. Additionally, the second angular peak is delayed, appearing at 80% of the gait cycle in the prototype versus 60% in the user, which can be attributed to actuator speed limitations.

Encouragingly, the prosthesis completes the inversion–eversion cycle in approximately 1.07 s, aligning closely with the average duration of natural gait. While finer kinematic details are not fully replicated, the system successfully reproduces the global temporal structure of this movement. Future improvements should prioritize increasing actuator responsiveness and enhancing mechanical articulation to better mimic the complexity of human ankle dynamics.

4.3 Abduction–adduction movement

The RMSE for abduction-adduction was 2.118, and the DTW distance reached 39.78, indicating greater discrepancy compared to dorsiflexion and eversion (Fig. 18). The warping path exhibits substantial temporal misalignments, indicating that the prosthesis struggles to accurately replicate transverse plane movements.

The prototype closely replicates the user's movement during the early gait phases, notably aligning with the initial negative peak at 20% of the cycle. However, in later subphases such as midstance and terminal stance, the prosthesis exhibits a clear phase shift: its peak occurs at 47%, while the user's occurs at 64%. This advancement likely stems from control system timing mismatches.

Although the system completes a functional gait cycle, deviations in timing and amplitude reflect limitations in control precision. The open-loop nature of the stepper motor, coupled with actuator speed constraints, contributes to these discrepancies. Variability in actuator response time further accentuates phase shifts.

A key difference is observed in the second positive peak, where the prototype reaches 7° with a steep slope, while the user remains at 0° with a gradual rise. This mismatch is primarily due to the absence of position feedback; the stepper motor operates at a constant, likely maximum, speed without real-time adjustment, thereby limiting accuracy.

Incorporating a feedback system, such as an encoder, would enhance movement fidelity by enabling adaptive speed control and phase synchronization. This improvement could significantly reduce timing and amplitude errors in abduction-adduction replication, bringing the prosthesis closer to natural ankle performance.

4.4 Reliability and durability of the prosthesis system

An exploratory reliability assessment of the electronic system was conducted using the MIL-HDBK-217F standard, which estimates failure rates based on empirical models. The total calculated failure rate was 1740×10^{-9} failures per hour, corresponding to an estimated reliability of 99.83% over 1000 h of use.

This estimate reflects performance under moderate conditions and does not account for mechanical wear in components such as the actuators and structural parts. For example, linear actuators are subject to repeated stress cycles that may reduce their efficiency over time, and the stepper motor may experience wear in its bearings or gears after extended use.

Since the prototype was tested in a controlled environment without user interaction, these estimates should be validated through long-term testing under real-world conditions. Accelerated life testing could also help identify potential failures under stress and provide a better understanding of the system's actual lifespan.

4.5 Comparison with existing transtibial prosthesis

The 2SPU-RU prototype introduces a parallel mechanism with three actively actuated degrees of freedom, allowing movement in the sagittal, frontal, and transverse planes. This setup aims to replicate natural ankle motion more accurately, thereby improving gait adaptability and balance. The design also distributes mechanical loads across multiple limbs and decouples motion in each plane, which may simplify control and reduce long-term wear. These features respond to

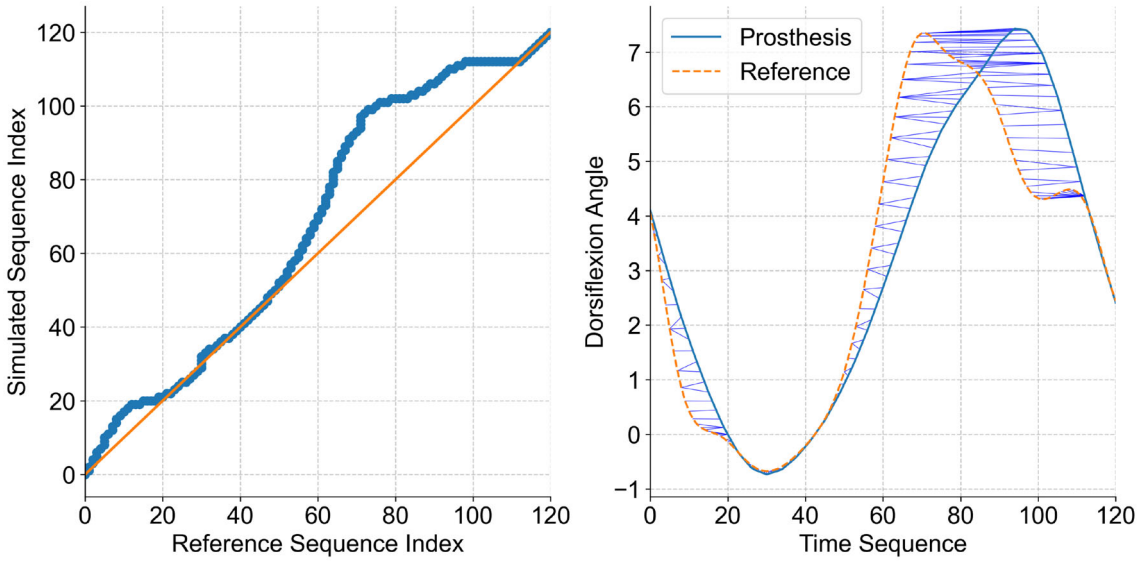

Fig. 17 Warping path, sequence, and alignment for inversion–eversion. Blue circle, warping path; red straight line, diagonal of the matrix; blue line, alignment

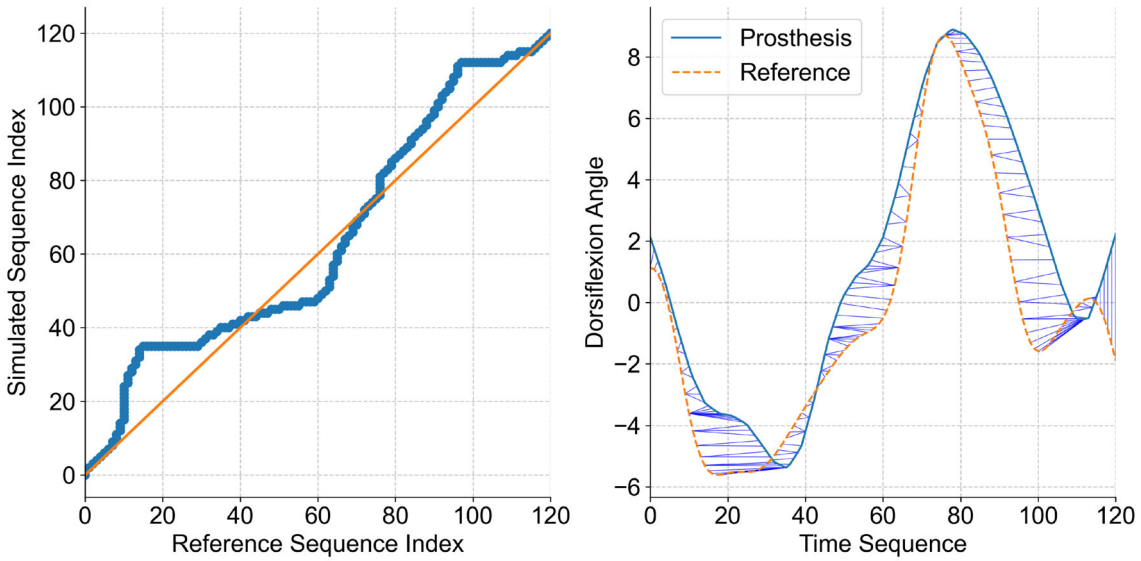

Fig. 18 Warping path, sequence, and alignment for abduction-adduction. Blue circle, warping path; red straight line, diagonal of the matrix; blue line, alignment

limitations found in current prosthetic systems, which often lack multi-directional mobility and rely on more complex actuation schemes.

To further illustrate the functional advantages of our 2SPU-RU prototype, Fig. 19 compares its motion capabilities with typical prosthetic designs, highlighting the three active degrees of freedom (DoF) across the sagittal, frontal, and transverse planes. This design sets our prototype apart from conventional prostheses, which typically offer one or two active planes of movement. Figure20 complements this by comparing the range of motion in dorsiflexion–plantarflexion and presenting a comparison of mechanism types and mass (kg) of active transtibial prostheses.

Table 2 compares our design with eleven transtibial prostheses from recent literature. It highlights differences in mechanism type (serial vs. parallel), number of active degrees of freedom (DoF), movement ranges, device mass, and the types of movements achieved. Our 2SPU-RU mechanism stands out as one of the few parallel designs and the only one capable of actively reproducing movements in all three anatomical planes. It also has the lowest structural weight

Table 2 Comparative overview of active transtibial prostheses: mechanism type, degrees of freedom, range of movement, mass, and actuated movements

Author (Year)	Type of mechanism	Type of prosthesis	Degrees of freedom (DoF)	Range of movement	Mass (kg)	Types of movements
Xiu et al. [34]	Parallel	Passive	2 DoF	DF-PF: 0 - 25 I-E: 11°	1.57 kg	DF-PF I-E (passive)
Madusanka et al. [17]	Serial	Active	3 DoF	DF-PF: 12 - 32 Ab-Ad: 20 - 35 I-E: 30 - 25°	3.8 kg	DF-PF Ab-Ad I-E (passive)
Rogers et al. [23]	Parallel	Active	2 DoF	DF-PF: 16.6° I-E: +22.3°	1.292 kg	DF-PF I-E
Wang, Yuan, Zhu, and Wang [33]	Serial	Active	1 DoF	DF-PF: +25°	1.3 kg	DF-PF I-E
Mazumder and Carloni (2020) [19]	Serial	Active	1 DoF	DF-PF: +10°	3 kg	DF-PF
Shehata, William, Hassan, and Ibrahim [30]	Serial	Semiactive	1 DoF	NE	NE	DF-PF
Hsieh et al. [10]	Serial	Active	2 DoF	DF-PF: 9° - 21° I-E: +13.5°	2.75 kg	DF-PF, I-E
Anderson, Hudak, Muir, and Aubin [3]	Serial	Active	2 DoF	NE	1.67 kg	DF-PF I-E
Gao, Liu, and Liao [6]	Serial	Active	2 DoF	DF-PF: 25° −45° (70°)	2.3 kg	DF-PF I-E
Sathsara, Widanage, Sooriyaperakasam, Ranaweera, and Gopura [29]	Serial	Active	1 DoF	DF-PF: 10° - 20° (30°)	1.4 kg	DF-PF (passive)
Heremans, Vijayakumar, Bouri, Dehez, and Ronsse [9]	Parallel	Active	1 DoF	NE	1.2 kg	DF-PF
2SPU-RU, 2025 (Proposed in this article)	Parallel	Active	3 DoF	DF-PF: 24° - 16° I-E: 26° - 13° Ab-Ad: 21° - 13°	0.5 kg (without electronic components)	DF-PF I-E Ab-Ad

DF:dorsiflexion, PF: plantarflexion, I: inversion , E: eversion, Ab: abduction, Ad: adduction

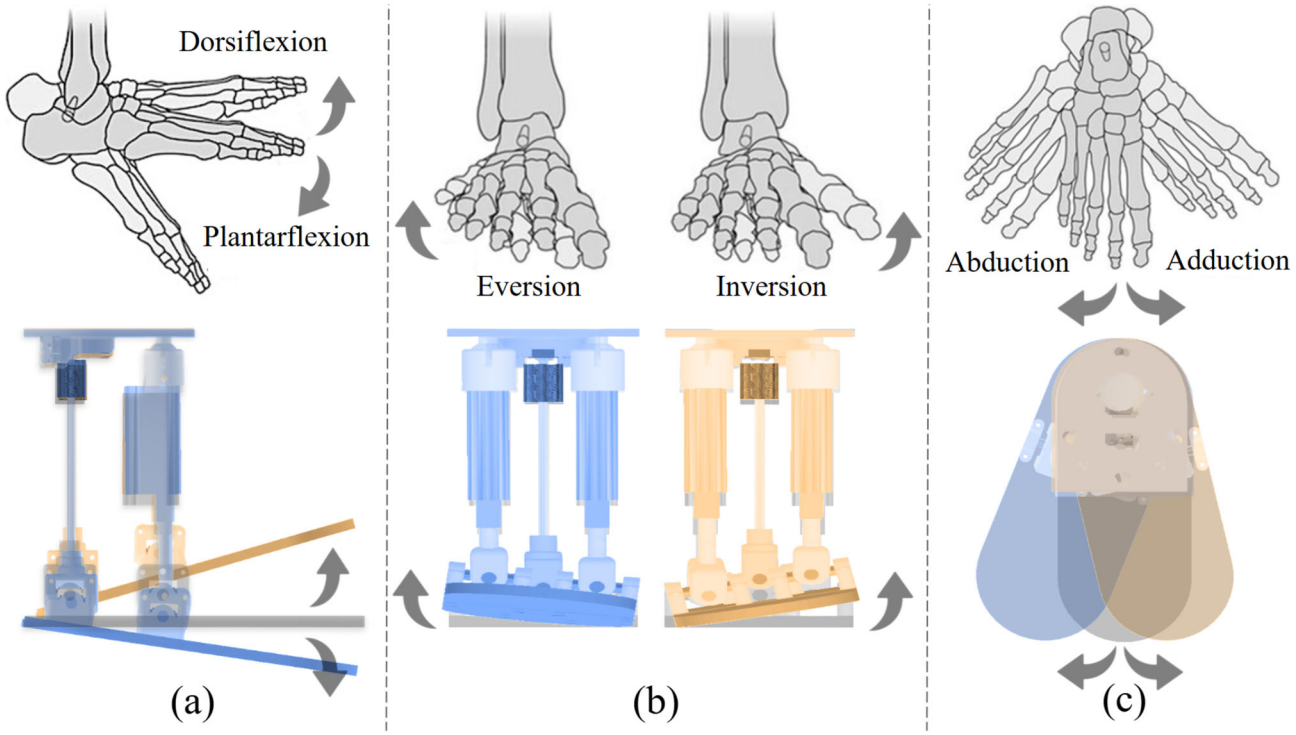

Fig. 19 Movements of the 2SPU-RU prototype: **a** dorsiflexion–plantarflexion in the sagittal plane, **b** inversion–eversion in the frontal plane, **c** abduction–adduction in the transverse plane

(0.5 kg, excluding electronics), suggesting an advantage in mobility and integration potential.

To better highlight the specific advantages of our system, Table 3 summarizes the main contributions of the 2SPU-RU prototype compared to the typical values found in the literature.

While most prostheses utilize serial mechanisms and typically actuate one or two planes, usually dorsiflexion/plantarflexion and sometimes inversion/eversion, our system is designed to reproduce the full range of ankle motion with active motion in all three planes. The prototype achieves comparable or better ranges of motion while maintaining a significantly lower mass.

However, these benefits come with trade-offs. The use of a parallel mechanism increases structural complexity and introduces new control challenges. Since this is an early-stage prototype (TRL 3), further development is needed to improve torque generation, ensure closed-loop control in all planes, and validate the system's performance under load.

In summary, this work does not simply adapt a rehabilitation mechanism to prosthetics. Instead, it takes advantage of the 2SPU-RU's structure, its ability to produce multi-directional motion, and handle forces more evenly to explore a potentially more functional and biomimetic solution for transtibial prosthesis users.

4.6 Future work

Future developments for the transtibial prosthesis prototype will focus on improving its mechanical performance, control architecture, and readiness for real-world application.

One priority is optimizing the selection of actuators, particularly by integrating options with higher torque and faster response. Additionally, lightweight actuation alternatives such as shape memory alloy (SMA) actuators could be explored to reduce the overall weight of the system while maintaining adequate force output [25]. These improvements aim to address current limitations in movement fidelity and peak torque generation.

Another area of development involves enhancing the control system. Future iterations may incorporate closed-loop feedback across all degrees of freedom, utilizing position sensors or encoders (such as Hall-effect sensors) to minimize trajectory deviations. Parameter sensitivity analysis and adaptive control algorithms could also be explored to improve system stability and responsiveness in variable gait conditions. While the integration of machine learning remains exploratory at this stage, it may offer tools for automatic tuning of control parameters based on real-time gait data in more advanced prototypes.

Additionally, future work will focus on validating and improving the energy efficiency of the system. Although no

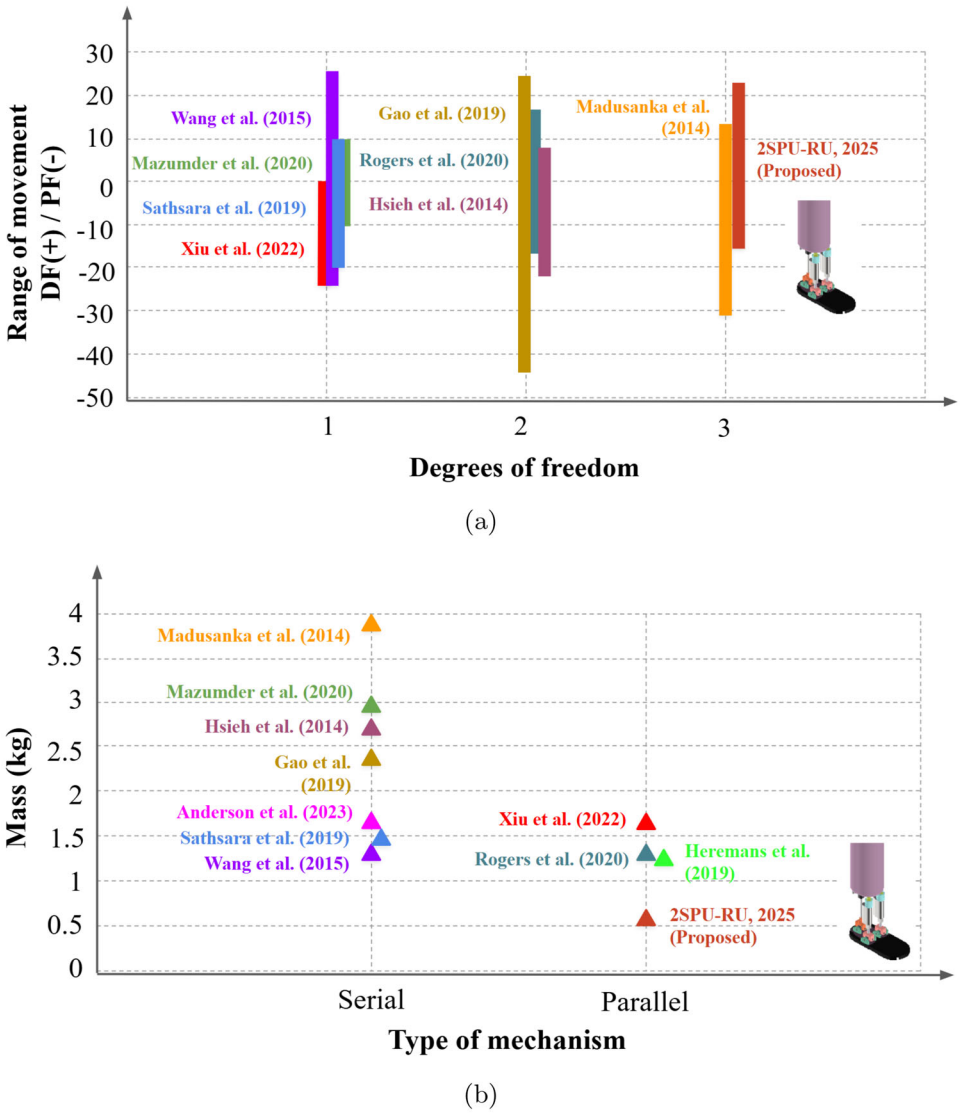

Fig. 20 Active transtibial prostheses comparison: **a** range of movement in dorsiflexion (DF) and plantarflexion (PF) vs degrees of freedom, **b** mass vs type of mechanism

detailed energy consumption testing has been performed on this initial prototype, the lightweight structure and reduced actuator count suggest the potential for improved energy efficiency in future iterations. Quantitative validation of energy use, including torque-per-watt metrics and battery endurance, is planned for higher-TRL evaluations once load-bearing capabilities and complete control integration are achieved. These studies will help establish the energy performance of the system, guiding further refinement to enhance actuator efficiency and overall energy consumption during gait.

It is essential to note that the current control system remains at an early stage of development, consistent with the prototype's Technology Readiness Level (TRL) 3. A more robust control system, incorporating closed-loop feedback for all axes and advanced control strategies, will be developed as part of TRL 5 and TRL 6. These stages will focus on refining the control architecture and addressing challenges such as system stability, robustness, and disturbance rejection in dynamic, real-world environments.

Validation in real-world settings is another critical step forward. Future testing will include walking on variable terrains and under dynamic conditions to assess the system's robustness and adaptability beyond laboratory environments.

Finally, clinical testing with transtibial amputees will be conducted to evaluate the functional performance and usability of the prosthesis. These trials will mark a key milestone in advancing the prototype toward higher technology readiness levels.

Table 3 Functional contributions of the 2SPU-RU robotic ankle prototype

Key metric	2SPU-RU prototype (TRL 3)	Typical range in literature (Table 2)	Remarks
Mechanism	Parallel	Mostly serial; only 3 of 11 devices employ parallel kinematics	Parallel architectures are still uncommon in ankle prostheses
Active DoF	3 (sagittal, frontal, transverse planes)	1–3; but simultaneously active in all three planes is absent in the surveyed prostheses	Our prototype is the only device in Table X that actively actuates all three anatomical planes
ROM (active)	DF–PF ≈ 40° (24° DF, 16° PF) I–E ≈ 39° (26° Inv, 13° Evers) Ab–Ad ≈ 34° (21° Abd, 13° Add)	DF–PF 20–70°, I–E up to 45°, Ab–Ad 20–25°	Our sagittal and frontal ROMs are within the mid–upper range; transverse ROM is comparable to the few devices that report it
Mass (without electronics)	0.5 kg	1.2–3.8 kg (median ≈ 1.8 kg)	Lowest structural mass in the survey; electronics/battery will increase weight, but starting chassis mass is advantageous

DF: dorsiflexion, PF: plantarflexion, I: inversion , E: eversion, Ab: abduction, Ad: adduction

5 Conclusion

This study presents the design exploration and functional validation of a transtibial prosthesis based on a 2SPU-RU parallel mechanism with three degrees of freedom. The prototype was developed to explore the feasibility of using parallel kinematic architectures to replicate ankle motion in the sagittal, frontal, and transverse planes.

Functional validation included gait-based kinematic replication using videogrammetry, force distribution analysis through pressure insoles, measurement of energy consumption, and an initial reliability assessment of the electronic system. The prototype successfully reproduced key gait subphases and general movement patterns, particularly in dorsiflexion–plantarflexion and inversion–eversion. However, limitations in actuator speed, torque output, and control fidelity resulted in noticeable deviations in timing and amplitude when compared to human reference data.

The analysis of ground interaction revealed that while the force distribution shape was preserved, peak amplitudes were significantly lower than those of a human user, consistent with the prototype's limited load-bearing capacity and torque generation capabilities. Energy consumption measurements revealed high-power demand during dorsiflexion, indicating the need for more efficient actuation strategies. Reliability calculations based on component failure rates suggest that the electronic system is likely to exhibit promising durability under moderate conditions. However, mechanical wear remains to be evaluated through long-term testing.

This exploratory study demonstrates the feasibility of using a 2SPU-RU configuration in transtibial prosthetics. While promising, the design must undergo additional refinement and validation before its practical deployment can be realized. Overall, this work demonstrates the feasibility and potential of applying parallel mechanisms to ankle prostheses through the development of a lightweight 2SPU-RU prototype with three actively actuated degrees of freedom. While the current design remains at a proof-of-concept stage (TRL 3), its ability to replicate ankle kinematics in all anatomical planes establishes a solid foundation for future advancement. Upcoming work will prioritize empirical validation of torque-angle behavior, dynamic gait performance, and load-handling capabilities. Additionally, real-world trials with transtibial amputees are planned to assess the usability, wearability, and clinical feasibility of the device. These next steps are essential to determine whether this architecture offers functional advantages over conventional prosthetic designs.

Funding Open access funding provided by Pontificia Universidad Catolica del Peru.

Data Availability All data are needed to evaluate the paper's conclusions. The authors may be requested to provide additional data or source code related to this paper.

Declarations

Conflict of interest The authors have no conflict of interest to declare that are relevant to the content of this article. The authors declare no conflict of interest.

References

1. Abarca VE, Elias DA (2023) A review of parallel robots: rehabilitation, assistance, and humanoid applications for neck, shoulder, wrist, hip, and ankle joints. Robotics 12:131. https://doi.org/10.3390/robotics12050131
2. Abarca VE, Elias DA (2024) Modeling and simulation of a 2spu-ru parallel mechanism for a prosthetic ankle with three degrees of freedom. Inventions 9:71. https://doi.org/10.3390/inventions9040071
3. Anderson AJ, Hudak YF, Muir BC, Aubin PM (2023) Design, control, and evaluation of a robotic ankle-foot prosthesis emulator. IEEE Trans Med Robot Bionics 5(3):741–752
4. Chai T, Draxler RR (2014) Root mean square error (rmse) or mean absolute error (mae)? Arguments against avoiding rmse in the literature. Geosci Model Dev 7:1247–1250. https://doi.org/10.5194/gmd-7-1247-2014
5. Chen X, Ji C, Guo Y, Zhang Z, Chen Z (2023) A novel 3-upu parallel ankle rehabilitation mechanism. Paper presented at international conference on mechanism and machine science, Yantai, China, 30 July–1 August 2022
6. Gao F, Liu Y, Liao W-H (2019) Implementation and testing of ankle-foot prosthesis with a new compensated controller. IEEE/ASME Trans Mechatron 24(4):1775–1784
7. Gonzales-Huisa OA, Oshiro G, Abarca VE, Chavez-Echajaya JG, Elias DA (2023) Emg and imu data fusion for locomotion mode classification in transtibial amputees. Prosthesis 5:1232–1256. https://doi.org/10.3390/prosthesis5040085
8. Greene MJ, Fischman Ekman Simões I, Lewis PR, Nichols KM, Adamczyk PG (2024) Non-backdrivable wedge cam mechanism for a semi-active two-axis prosthetic ankle. Prosthesis 6:683–707. https://doi.org/10.3390/prosthesis6030049
9. Heremans F, Vijayakumar S, Bouri M, Dehez B, Ronsse R (2019) Bio-inspired design and validation of the efficient lockable spring ankle (elsa) prosthesis. In: 2019 IEEE 16th international conference on rehabilitation robotics (icorr), pp 411–416
10. Hsieh TH, Song H, Shu T, Qiao J, Yeon SH, Carney M, Herr H (2024) Design, characterization, and preliminary assessment of a two-degree-of-freedom powered ankle–foot prosthesis. Biomimetics (Basel) 9:76. https://doi.org/10.3390/biomimetics9020076
11. Huamanchahua D, Osores-Aguilar D, Leon-Sales VA, Valenzuela-Lino YS, Huallanca-Escalera H (2022) Transtibial electromechanical prosthesis based on a parallel robot: a innovate review. Paper presented at 2022 IEEE international IOT, electronics and mechatronics conference (IEMTRONICS), 1–4 June 2022
12. Ismawan AR, Ismail R, Prahasto T, Ariyanto M, Setiyana B (2022) A review of existing transtibial bionic prosthesis: mechanical design, actuators and power transmission. J Biomed Eng 1:65–72. https://doi.org/10.14710/jbiomes.2021.v1i2.65-72
13. Klein JG, Voglewede PA (2018) Stiffness control of an active transtibial prosthesis. Paper presented at 42nd mechanisms and robotics conference, 26–29 August 2018
14. Lee H-S (2019) Application of dynamic time warping algorithm for pattern similarity of gait. J Exercise Rehabil 15(4):526–530. https://doi.org/10.12965/jer.1938384.192
15. Lemoyne R (2015) Advances regarding powered prosthesis for transtibial amputation. J Mech Med Biol 15:1530001. https://doi.org/10.1142/S021951941530001X
16. Li J, Fan W, Dong M, Rong X (2020) Research on control strategies for ankle rehabilitation using parallel mechanism. Cognit Comput Syst 2:105–111. https://doi.org/10.1049/ccs.2020.0012
17. Madusanka D, Wijayasingha L, Sanjeevan K, Ahamed M, Edirisooriya J, Gopura R (2014) A 3dof transtibial robotic prosthetic limb. In 7th International conference on information and automation for sustainability, pp 1–6
18. Mathijssen G, Cherelle P, Lefeber D, Vanderborght B (2013) Concept of a series-parallel elastic actuator for a powered transtibial prosthesis. Actuators 2:59–73. https://doi.org/10.3390/act2030059
19. Mazumder A, Carloni R (2020) Mechatronic design and adaptive control of a lower limb prosthesis. In: 2020 8th IEEE ras/embs international conference for biomedical robotics and biomechatronics (biorob), pp 446–451
20. Miller JD, Beazer MS, Hahn ME (2013) Myoelectric walking mode classification for transtibial amputees. IEEE Trans Biomed Eng 60(2745–2750):1. https://doi.org/10.1109/TBME.2013.2264466
21. Nguyen Phu S, Essomba T, Idram I, Lai JY (2019) Kinematic analysis and evaluation of a hybrid mechanism for computer assisted bone reduction surgery. Mech Sci 10:589–604. https://doi.org/10.5194/ms-10-589-2019
22. Pană CF, Manta LF, Vladu IC, Cismaru SI, Petcu FL, Cojocaru D, Bîzdoacă N (2022) The design of a smart lower-limb prosthesis supporting people with transtibial amputation—a data acquisition system. Appl Sci (Basel) 12:6722. https://doi.org/10.3390/app12136722
23. Rogers EA, Carney ME, Yeon SH, Clites TR, Solav D, Herr HM (2020) An ankle-foot prosthesis for rock climbing augmentation. IEEE Trans Neural Syst Rehabil Eng 29:41–51
24. Rosenblatt NJ, Bauer A, Rotter D, Grabiner MD (2014) Active dorsiflexing prostheses may reduce trip-related fall risk in people with transtibial amputation. J Rehabil Res Dev 51:1229–1242. https://doi.org/10.1682/JRRD.2014.01.0031
25. Sadeghi M, Abbasimoshaei A, Kitajima Borges JP, Kern TA (2024) Numerical and experimental study of a wearable exo-glove for telerehabilitation application using shape memory alloy actuators. Actuators 13:409. https://doi.org/10.3390/act13100409
26. Sarajchi M, Kenan Al-Hares M, Sirlantzis K (2021) Wearable lower-limb exoskeleton for children with cerebral palsy: a systematic review of mechanical design, actuation type, control strategy, and clinical evaluation. IEEE Trans Neural Syst Rehabil Eng 29(29):2695–2720. https://doi.org/10.1109/TNSRE.2021.3136088
27. Sarajchi M, Sirlantzis K (2023) Pediatric robotic lower-limb exoskeleton: an innovative design and kinematic analysis. IEEE Access 11(11):115219–115230. https://doi.org/10.1109/ACCESS.2023.3325211
28. Sarajchi M, Sirlantzis K (2025) Evaluating the interaction between human and paediatric robotic lower-limb exoskeleton: a model-based method. IJIRA 9(1):47–61. https://doi.org/10.1007/s41315-025-00421-x
29. Sathsara AP, Widanage KN, Sooriyaperakasam N, Ranaweera R, Gopura R (2019) A hybrid powering mechanism for a transtibial robotic prosthesis. In: 2019 Moratuwa engineering research conference (mercon), pp 447–453

30. Shehata E, William MY, Hassan A, Ibrahim K (2024) Development of powered semi-active ankle-foot prosthetic with fuzzy logic-pi controller. JES J Eng Sci 52(1):1–15
31. Song M, Guo S, Wang X, Qu H (2020) Dynamic analysis and performance verification of a novel hip prosthetic mechanism. Chin J Mech Eng. https://doi.org/10.1186/s10033-020-0436-5
32. Wang Q, Yuan K, Zhu J, Wang L (2015) Walk the walk: a lightweight active transtibial prosthesis. IEEE Robot Autom Mag 22:80–89. https://doi.org/10.1109/MRA.2015.2408791
33. Wang Q, Yuan K, Zhu J, Wang L (2015) Walk the walk: a lightweight active transtibial prosthesis. IEEE Robot Autom Mag 22(4):80–89
34. Xiu H, Han Y, Wang X, Zhang Y, Liang W, Wei G, Ren L (2022) Design, development, and clinical validation of a two degrees of freedom compliant ankle-foot prosthesis based on a 4–4r parallel mechanism. Mech Mach Theory 172:104818
35. Zhang J, Ma Z, Wei J, Yang S, Liu C, Guo S (2023) A novel evaluation index and optimization method for ankle rehabilitation robots based on ankle-foot motion. J Biomech Eng 145:051006. https://doi.org/10.1115/1.4056479
36. Zuo S, Li J, Dong M, Zhou X, Fan W, Kong Y (2020) Design and performance evaluation of a novel wearable parallel mechanism for ankle rehabilitation. Front Neurorobot. https://doi.org/10.3389/fnbot.2020.00009